Electronic Supplementary Material (ESI) for Inorganic Chemistry Frontiers.

Supporting Information for

A Quantitative Single-Nanowire Study on the Plasmonic Enhancement for the Upconversion Photoluminescence of Rare-Earth-Doped Nanoparticles

Xin Su, Li-Wei Chen, Zhejiaji Zhu, Jiani Li, Nan Zhang, Tong-An Bu, Yu-Chen Hao, Wen-Yan Gao, Di Liu, Si-Qian Wu, Zi-Long Yu, Hui-Zi Huang, and An-Xiang Yin*

Ministry of Education Key Laboratory of Cluster Science, Beijing Key Laboratory of Photoelectronic/Electrophotonic Conversion Materials, Advanced Technology Research Institute (Jinan), School of Chemistry and Chemical Engineering, Beijing Institute of Technology, Beijing 100081, China.

Chemicals

The rare earth (RE) oxides (Gd_2O_3 (99.99%), Yb_2O_3 (99.99%), Er_2O_3 (99.99%), Tm_2O_3 (99.99%) and Y_2O_3 (99.99%)), trifluoroacetic acid (CF_3COOH, 99%), oleylamine (OM, $C_{18}H_{37}N$, 90%), trifluoroacetic acid sodium salt (CF_3COONa, 98%), and copper chloride dihydrate ($CuCl_2.2H_2O$, 98%) were obtained from Energy Chemical (China); Oleic acid (OA, $C_{18}H_{34}O_2$, 90%), nitrosonium tetrafluoroborate ($NOBF_4$, 98%), and ethylene glycol (EG, $(CH_2OH)_2$, 99%) were purchased from Alfa Aesar (USA); 1-octadecence (ODE, $C_{18}H_{36}$, 90%), polyvinylpyrrolidone (PVP, $(C_6H_9NO)_n$, M_W=55000), and silver nitrate ($AgNO_3$, 99.8%) were supplied by Aladdin (China); 3-Mercaptopropionic acid (MPA, $C_3H_6O_2S$, 99%) was purchased from Aldrich; Hydrogen peroxide (H_2O_2, 30%) was supplied by Xi Long (China); Ammonia ($NH_3 \cdot H_2O$, 25%–28%) was purchased from Macklin (China); Cyclohexane (C_6H_{12}, AR) and N,N-Dimethylformamide (DMF, C_3H_7NO, AR) were from Beijing chemical works (China); Toluene (C_7H_8, AR), ethanol (C_2H_5OH, AR), and acetone (CH_3COCH_3, AR) were from Beijing Chemical Reagent Co. Ltd. (China). All chemical reagents were used without further purification.

Preparation of upconversion nanoparticles (UCNPs) with Tm/Er-doped cores and undoped shells with tunable thicknesses. Firstly, RE trifluoroacetates were obtained by dissolving the corresponding RE oxides in the trifluoroacetic acid.[1] The $NaGdF_4$:Yb,(Tm/Er)@$NaYF_4$ (donated as Tm/Er-doped UCNPs) was prepared by a step-by-step process.[2] Firstly, the β-$NaGdF_4$:Yb,(Tm/Er) (donated as β-Tm/Er) was synthesized by the high-temperature thermolysis method under oxygen-free procedures. Typically, $RE(CF_3COO)_3$ (1 mmol, Gd/Yb/Tm = 49/50/1 or Gd/Yb/Er = 78/20/2) and CF_3COONa (1 mmol) were added into a 100 mL three-necked flask containing 40 mmol of mixture (OA/OM/ODE = 1/1/2). The slurry was heated to 110 °C for 30 min under vacuum and then heated to 310 °C for 19 min under N_2 protection. After cooling to room temperature (RT), the precipitates were collected by centrifugation and dispersed in 10 mL of cyclohexane. A 5 mL amount of as-prepared nanoparticle colloidal solution (nominal 0.5 mmol) was added in OA/ODE mixture (40 mmol, molar ratio = 1/1), containing CF_3COONa (0.5 mmol) and $RE(CF_3COO)_3$ (0.5 mmol, Gd/Yb/Tm = 49/50/1 or Gd/Yb/Er = 78/20/2). The removal of cyclohexane, water, and oxygen was required before heating to 310 °C under N_2 atmosphere. The reaction was maintained at 310 °C for 30 min, and the aftertreatments were identical to that in the first step. Finally, the Tm/Er-doped

UCNPs were obtained by the following process. 2.5 mL of as-prepared β-Tm/Er solution (nominal 0.25 mmol) was added into 40 mmol of OA/ODE mixture (molar ratio= 1/1) containing precursors of shell (0.25 mmol of CF_3COONa and 0.25 mmol of $Y(CF_3COO)_3$). Reaction conditions and aftertreatments were identical to those in the phase transition process. Tm/Er-doped UCNPs with different shell thicknesses were obtained by following identical procedures to those above-mentioned, except for using different amounts of shell precursors (0.5, 0.75, 1, 1.5, 2, 3 mmol). The products were redispersed in 10 mL of cyclohexane. In addition, Tm-doped UCNPs with different Tm^{3+} doping concentrations (e.g., 0.5% and 1.5%) was also prepared under the similar conditions.

Surface modifications of UCNPs. Surface modifications of UCNPs were achieved by a ligand-exchange reaction followed by the MPA attachment.[3] Typically, 2 mL of as-prepared hydrophobic UCNPs was added into the solution containing 5 mL of cyclohexane and 5 mL of DMF at RT. Then, 50 mg of $NOBF_4$ was added to the mixture and stirred for 1 h. The nanoparticles were then purified by precipitation with the addition of toluene. Finally, the products were dispersed in 2 mL of DMF. For MPA-modified UCNPs (MPA-UCNPs), 0.5 mL of as-prepared hydrophilic UCNPs was incubated with MPA in DMF (0.05 mM, 1 mL) for 12 h under continuous vibration with a shaker. After the reaction, the nanoparticles were collected by centrifugation at 14900 rpm for 15min and washed three times with DMF. Finally, the MPA-UCNPs were dispersed in 2 mL of DMF.

Synthesis of AgNWs. AgNWs were synthesized by the reported PVP-assisted polyol process with minor modifications.[4] Firstly, PVP (Mw=55000, 0.8 g) was dissolved in 100 mL of EG. Then, $AgNO_3$ (0.1 g) was added to 10 mL of EG with PVP under stirring. When $AgNO_3$ dissolved completely, $CuCl_2 \cdot 2H_2O$ (3.3 mM in EG, 160 μL) was added under vigorous stirring. After that, the solution was heated in an oil bath at 130 °C and kept undisturbed for 3 h. After cooling down to RT, the products were rinsed three times with acetone and ethanol. Finally, the PVP-modified AgNWs (PVP-AgNWs) were dispersed in 10 mL of DMF for further use.

Assembly of MPA-UCNPs with PVP-AgNWs. UCNPs/AgNWs were prepared by the MPA-assisted chemical method. Typically, 0.6 mL of as-prepared PVP-AgNWs was diluted to 6 mL with DMF and sonicated for 5 min. Meantime, 0.5 mL

of MPA-UCNPs was also diluted to 5 mL with DMF. Then, different amounts of MPA-UCNPs (2, 1.5, 1, 0.7, 0.5, 0.1 mL) were mixed with 1 mL of diluted PVP-AgNWs solution, and the pure DMF was subsequently added to the mixture to reach a final volume of 3 mL. After shaking at RT for 12 h, the products were collected by centrifugation and washed three times with DMF. Finally, the products were redispersed in 2 mL of DMF. Similarly, UCNPs/AgNWs with tunable distances between the AgNWs surfaces and the UCPL cores were obtained by mixing AgNWs with MPA-UCNPs with different shell thicknesses at the same experimental conditions. Moreover, UCNPs(Tm)/AgNWs with different Tm^{3+} doping concentrations were prepared by mixing AgNWs with MPA-UCNPs(Tm) with different Tm^{3+} doping ratios at the similar conditions.

Selective etching of AgNW in UCNPs/AgNWs. AgNWs in nanohybrids were moved away by using the mixture of $NH_3 \cdot H_2O$ and H_2O_2.[5] Firstly, a DMF droplet of UCNPs/AgNWs was randomly deposited on SiO_2(300 nm)/Si substrate with markers via solvent evaporation method. Then, $NH_3 \cdot H_2O$ (2 M, 2.5 mL) and H_2O_2 (2 M, 2.5 mL) were mixed in a 20 mL glass flask. Next, after optical measurements, the substrate with UCNPs/AgNWs was wholly immersed in the mixture and kept undisturbed for 8 h at 4 °C. Then, the substrate was placed in a new mixture for another 2 h. After that, the substrate was taken out and washed with pure DMF. Finally, the substrate was dried in the open air at RT for further tests.

Characterizations. Transmission electron microscopy (TEM) and high-resolution TEM (HRTEM) measurements were performed on a JEM-2100 (JEOL, Japan) transmission electron microscope operating at 200 kV. Scanning electron microscopy (SEM) measurements were performed on a Supra-55 (ZEISS, Germany) field emission SEM microscope. Fourier Transform infrared (FTIR) spectra were collected on a Bruker ALPHA spectrometer (resolution: 4 cm^{-1}).

Figures and Tables

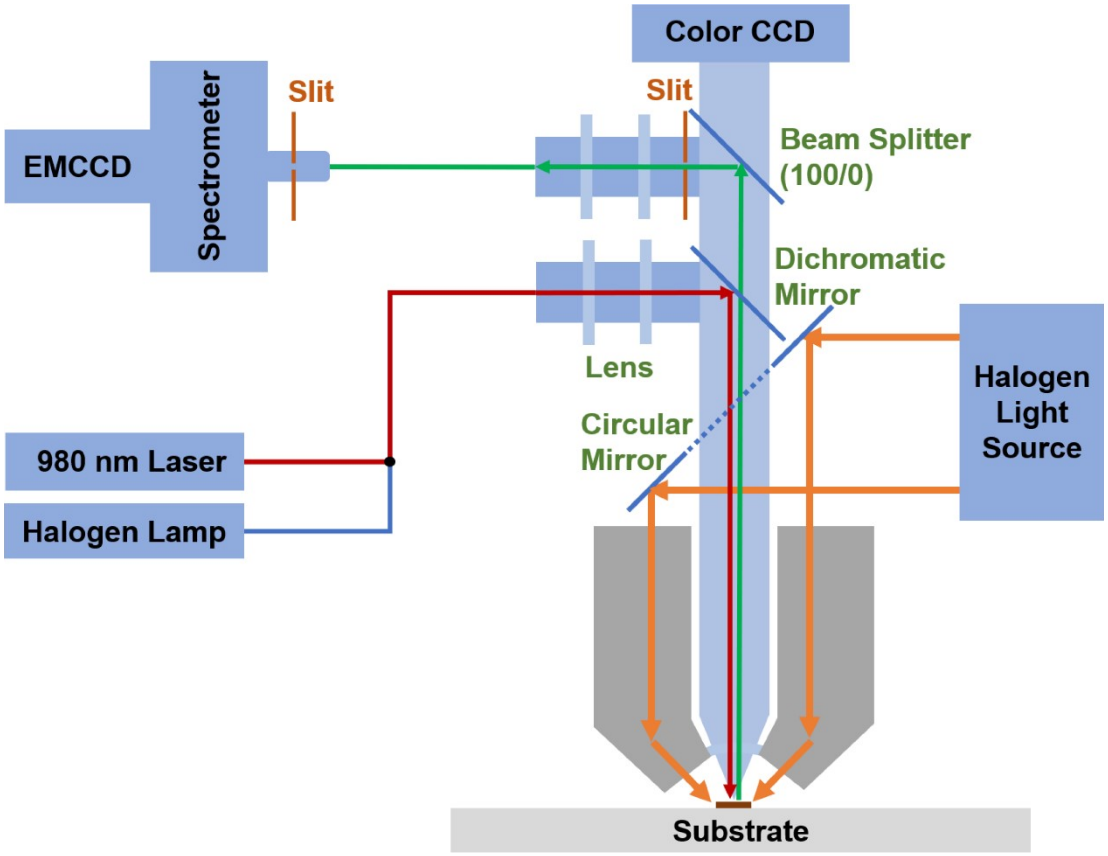

Figure S1. Scheme illustration for an optical microscope system. A quartz-tungsten-halogen lamp (100 W, Leica) was used to capture the dark field (DF) images of AgNWs and a diode 980 nm laser (5 W, Hi-Tech Optoelectronics Co., Ltd. China) was used to stimulate the UCNPs. A 5× objective lens with a numerical aperture (NA) of 0.15 and a 50× objective lens with the NA of 0.55 were used to focus the laser beam onto the samples. The accurate positioning of specific sample was realized by the halogen lamp with the help of the markers on the silica wafers. Moreover, the selective illumination and spectrum acquisition of the single nanowire were achieved by adjusting the spot sizes of the incident light, the diameter of the optical fiber, and the slit of the spectrometer, avoiding the interferences from nearby samples. The scattering and emission spectra of UCNP/AgNW on the single-nanowire scale were collected by the same lens and filtered the excitation light by a short pass filter (FESH0750, THORLABS) before entering the spectrometer (iHR550, Horiba) and electron-multiplying charge-coupled device (EMCCD, synapse EM, Horiba), which coupled with the microscope (DM2700M, Leica) by optical fibers.

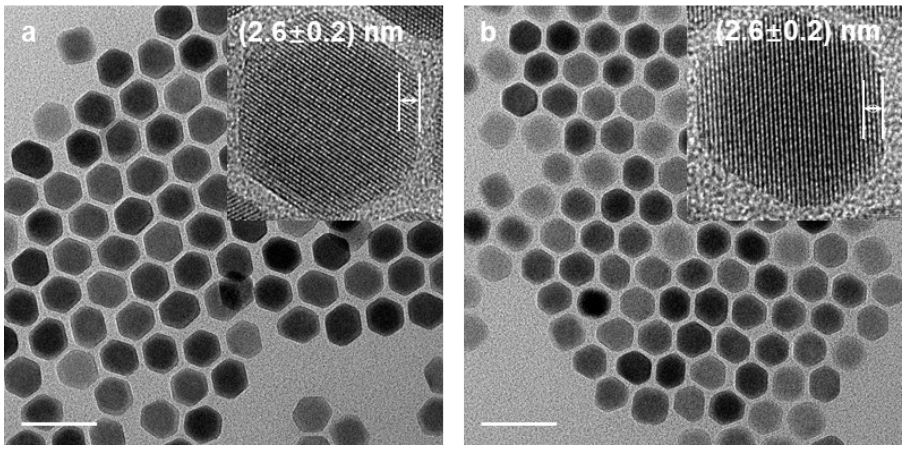

Figure S2. **TEM images of Tm-doped UCNPs with different Tm^{3+} doping concentrations:** (a) 0.5%Tm@2.6 NPs, (b) 1.5%Tm@2.6 NPs. Scale bars:50 nm.

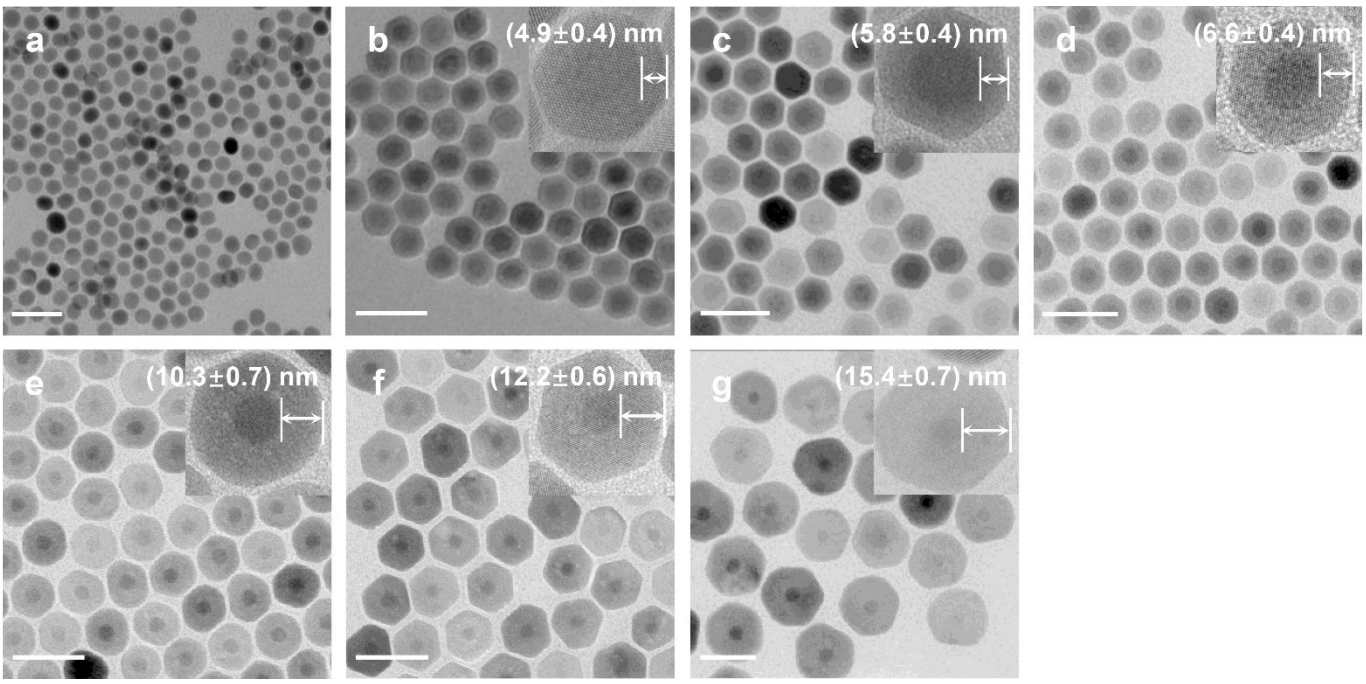

Figure S3. TEM images of Tm-doped UCNPs. (**a**) Uncoated *β*-Tm NPs. (**b**–**g**) Tm-doped cores with varied $NaYF_4$ shell thicknesses from 4.9 to 15.4 nm: (**b**) 4.9 nm, (**c**) 5.8 nm, (**d**) 6.6 nm, (**e**) 10.3 nm, (**f**) 12.2 nm, (**g**) 15.4 nm. Inset in (**b**–**g**): the corresponding HRTEM images for the UCNPs with the average shell thicknesses indicated. Scale bars: 50 nm.

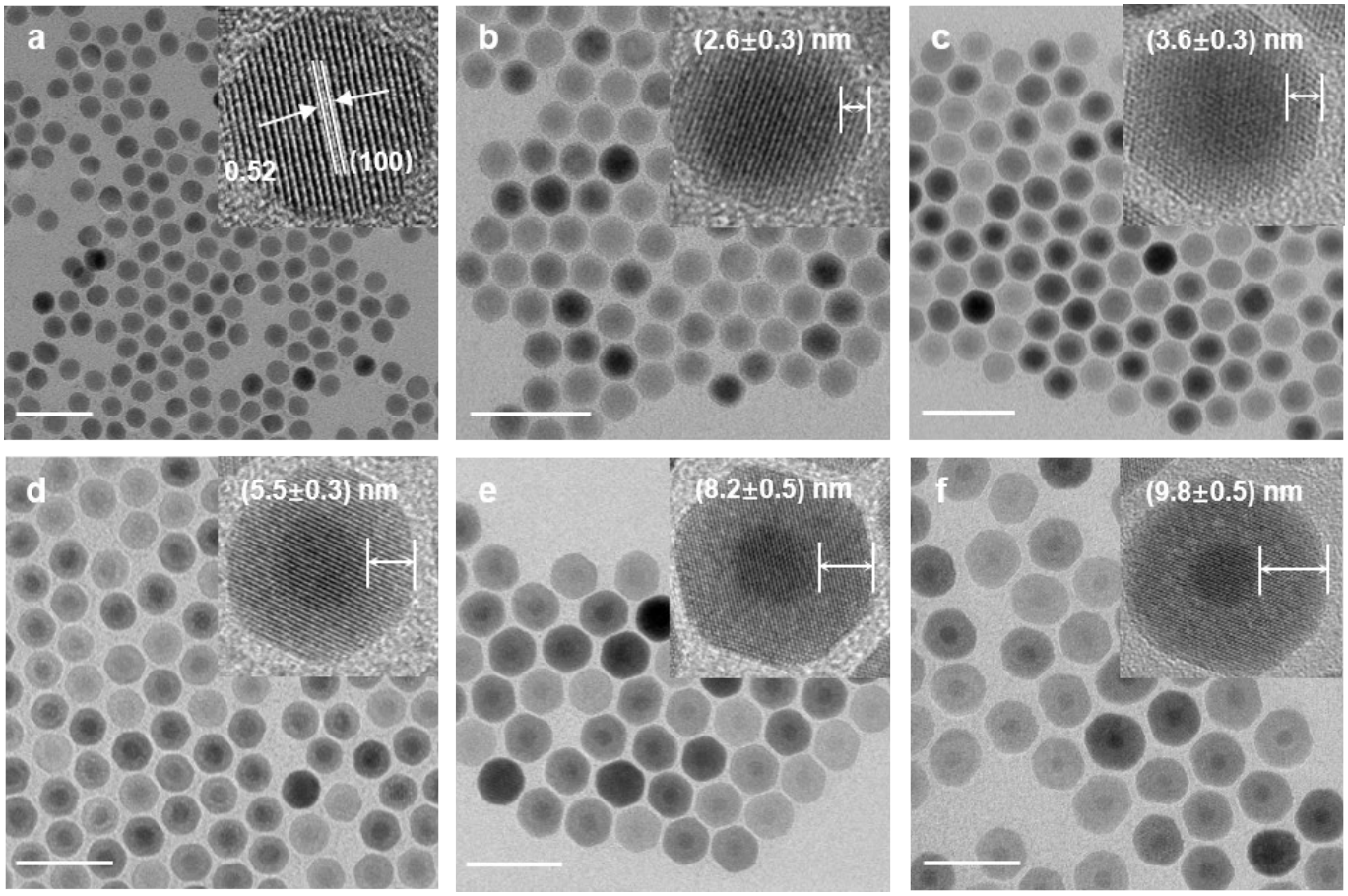

Figure S4. TEM images of Er-doped UCNPs. (**a**) Uncoated β-Er NPs. Inset: the corresponding HRTEM image. (**b**–**f**) Er-doped cores with varied $NaYF_4$ shell thicknesses from 2.6 to 9.8 nm: (**b**) 2.6 nm, (**c**) 3.6 nm, (**d**) 5.5 nm, (**e**) 8.2 nm, (**f**) 9.8 nm. Inset in (**b–f**): the corresponding HRTEM images for the UCNPs with the average shell thicknesses indicated. Scale bars: 50 nm.

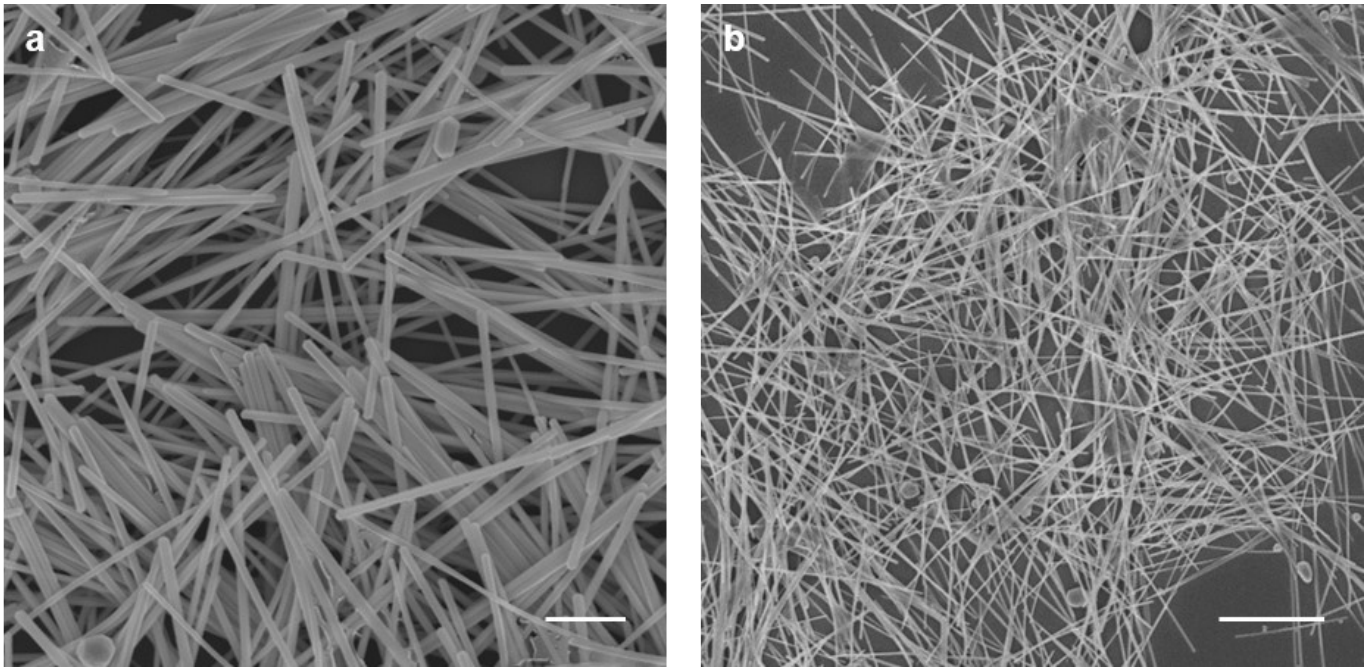

Figure S5. SEM images of AgNWs. Scale bars: (**a**) 1 μm, (**b**) 4 μm.

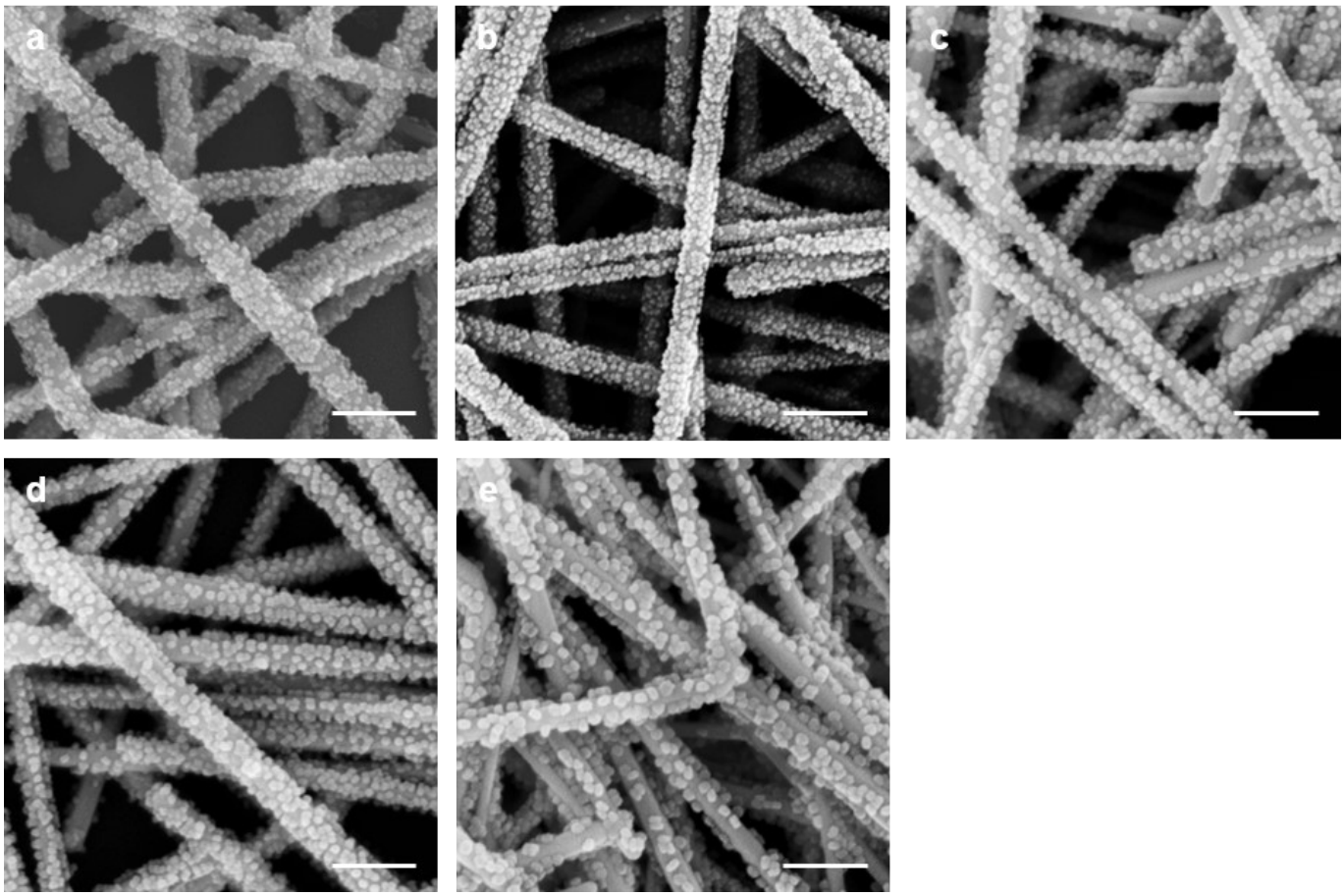

Figure S6. SEM images of Tm-doped UCNPs/AgNWs. (**a**) Uncoated β-Tm/AgNWs, (**b**–**e**) Tm-doped UCNPs/AgNWs with varied $NaYF_4$ shell thicknesses: (**b**) 4.9 nm, (**c**) 5.9 nm, (**d**) 6.6 nm, (**e**) 12.2 nm. Scale bars: 300 nm.

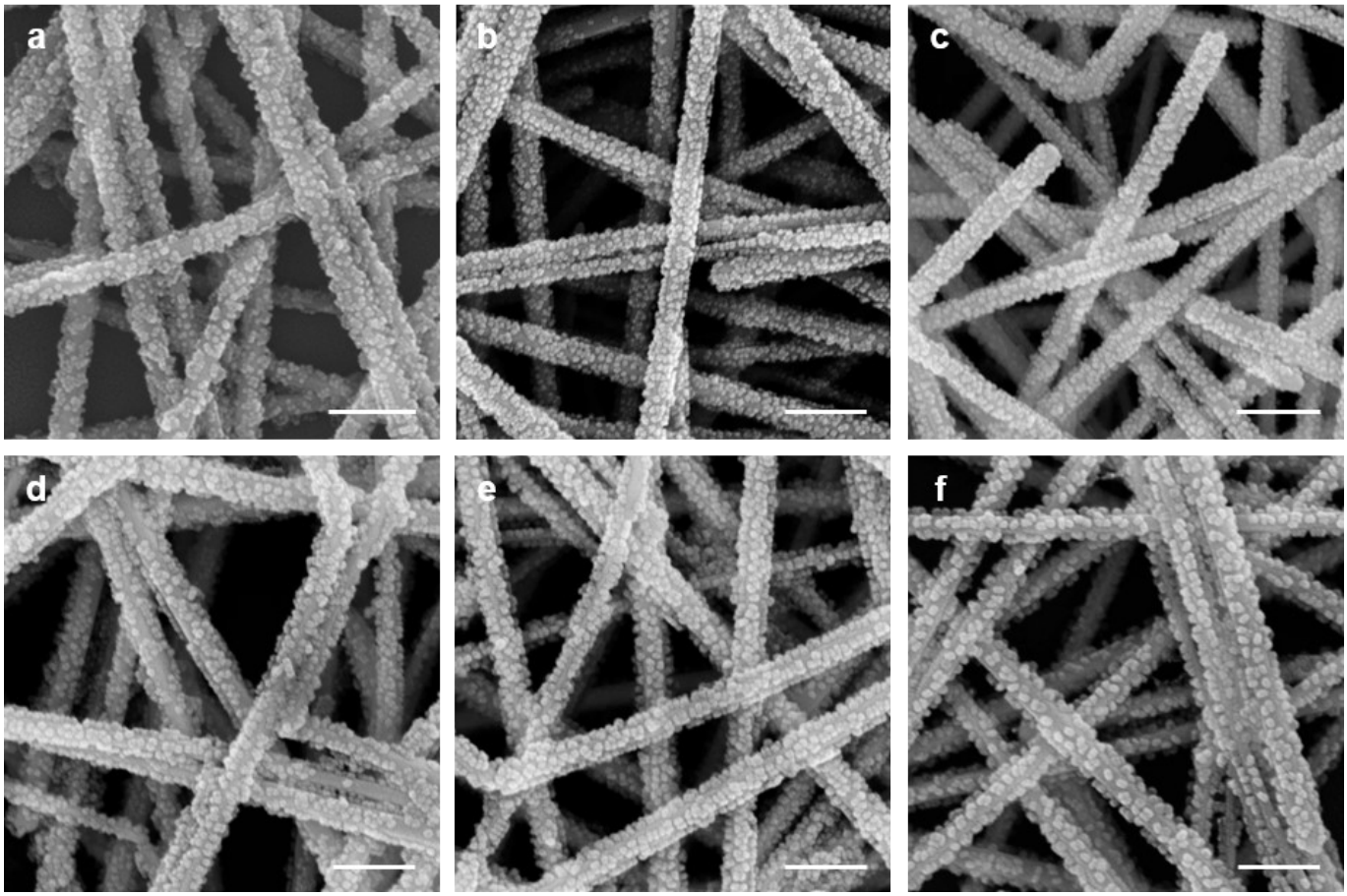

Figure S7. SEM images of Er-doped UCNPs/AgNWs. (**a**) Uncoated β-Er/AgNWs, (**b**–**f**) Er-doped UCNPs/AgNWs with different $NaYF_4$ shell thicknesses: (**b**) 2.6 nm, (**c**) 3.6 nm, (**d**) 5.5 nm, (**e**) 8.2 nm, (**f**) 9.8 nm. Scale bars: 300 nm.

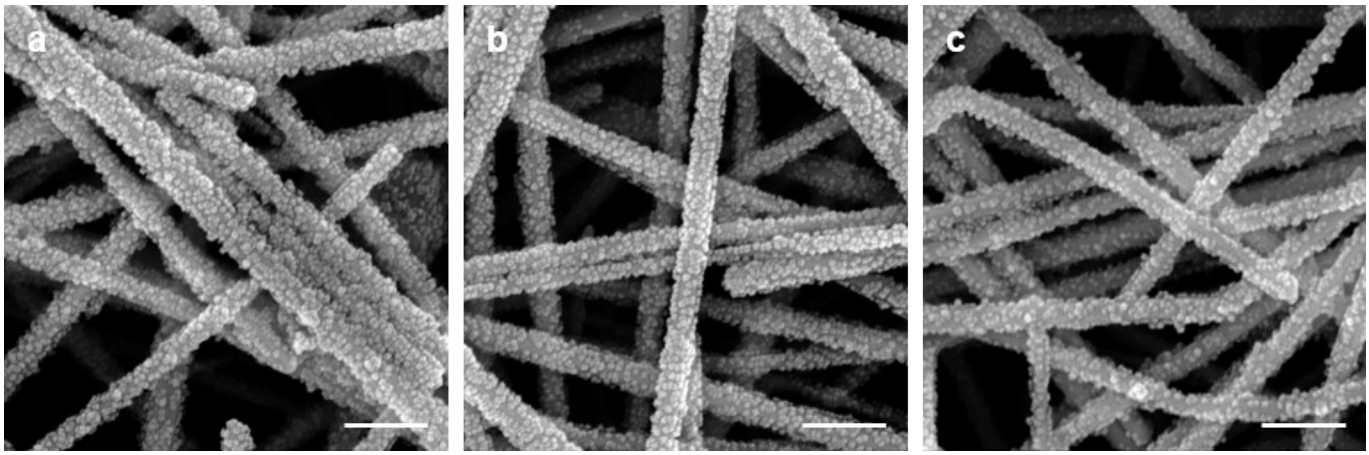

Figure S8. SEM images of Er@2.6/AgNWs with tunable surface coverages of Er@2.6 NPs on AgNWs. Scale bars: 300 nm.

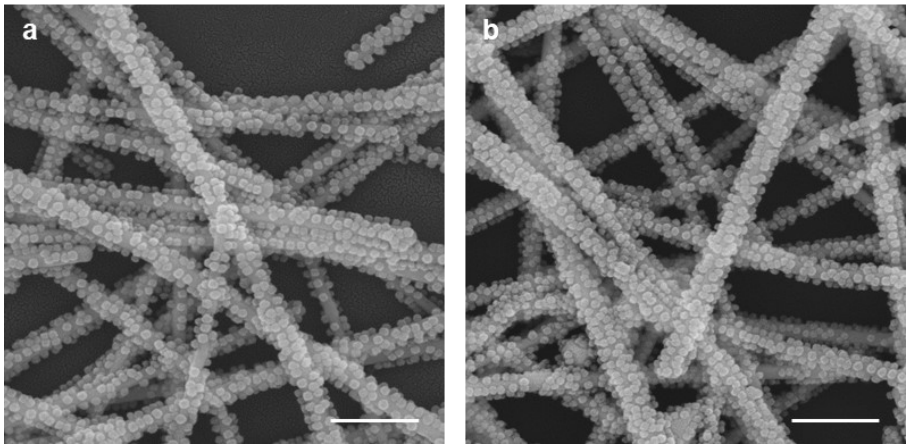

Figure S9 SEM images of UCNPs(Tm)/AgNWs with different Tm^{3+} doping concentrations: (a) 0.5%Tm@2.6/AgNWs, (b) 1.5%Tm@2.6/AgNWs. Scale bars:300 nm.

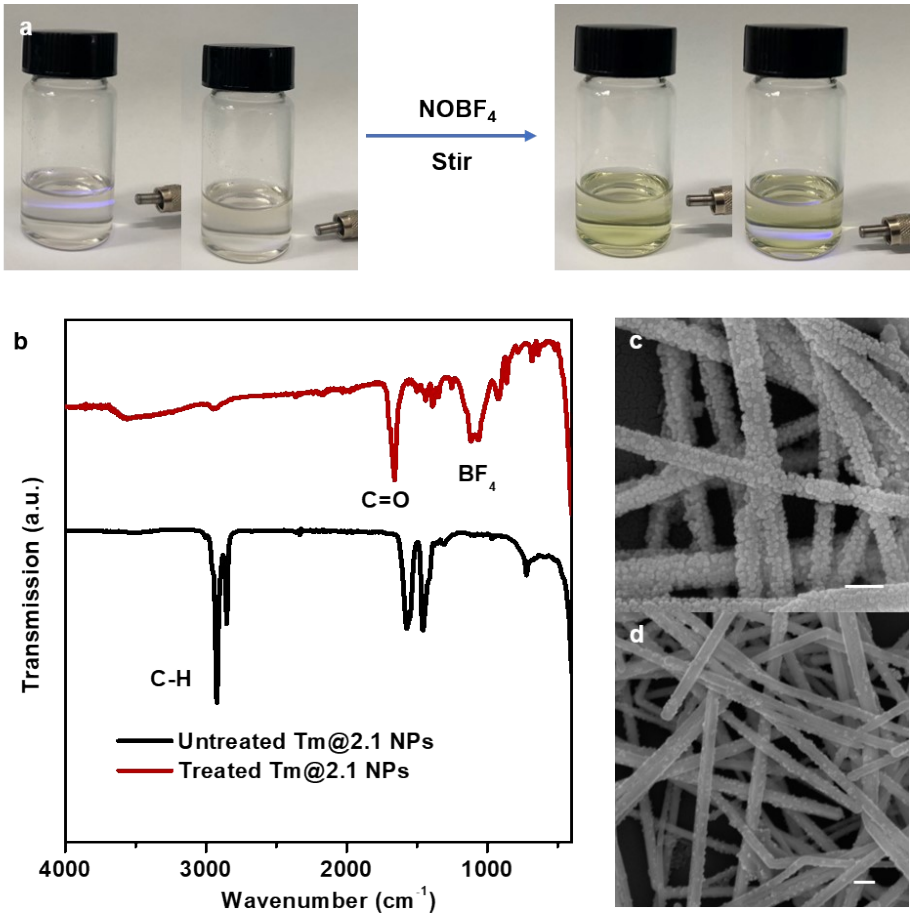

Figure S10. Surface modification of Tm@2.1 NPs and control experiments for Tm@2.1/AgNWs in the presence and absence of MPA. (**a**) Photographs of colloidal dispersions and visible upconversion photoluminescence of Tm@2.1 NPs before (left) and after (right) $NOBF_4$ treatment, respectively. (**b**) FTIR spectra for Tm@2.1 NPs before (black) and after (red) $NOBF_4$ treatment. (**c**, **d**) SEM images of Tm@2.1/AgNWs synthesized in the presence (**c**) and absence (**d**) of MPA. Scale bars: 200 nm.

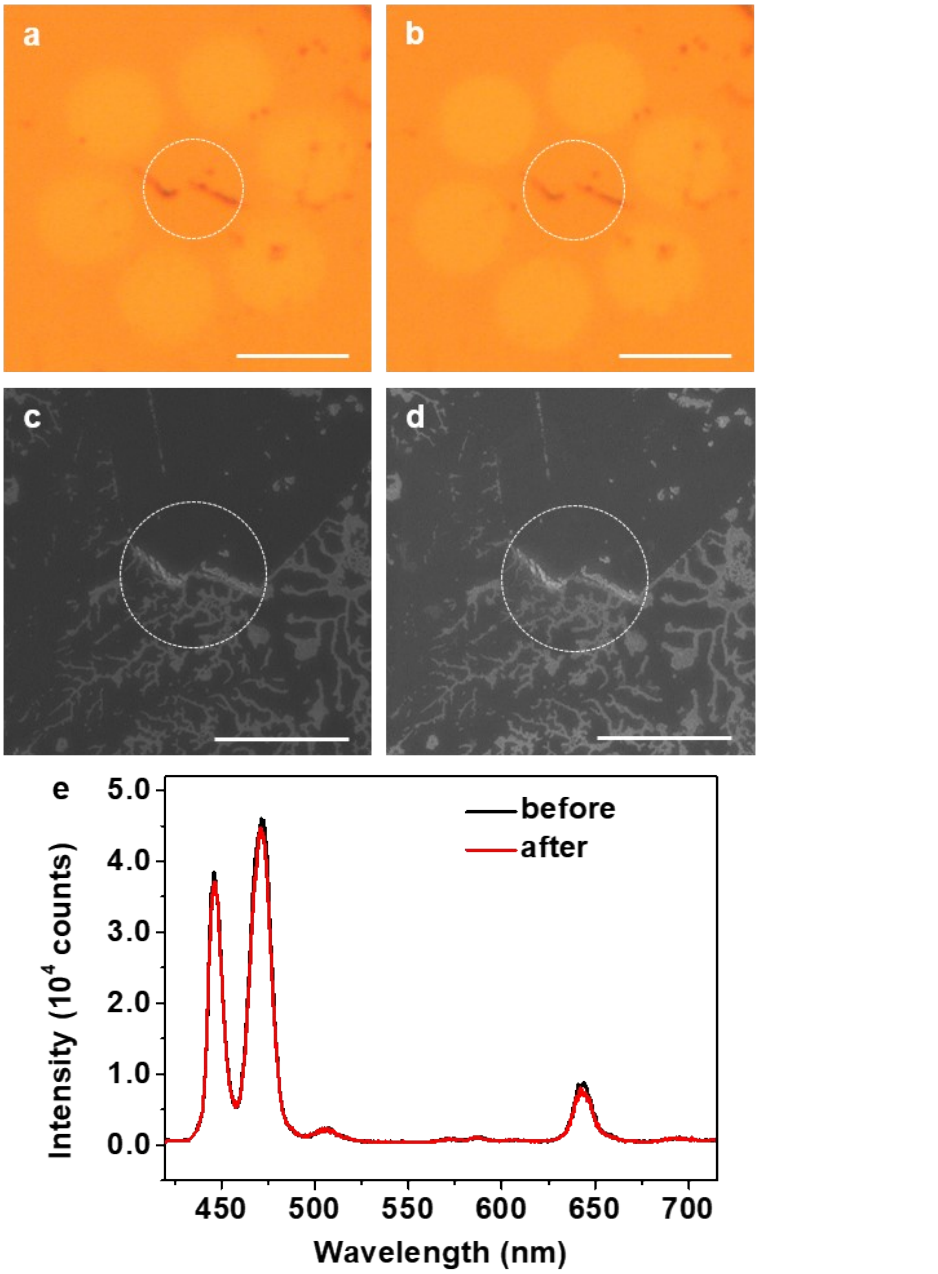

Figure S11. The etching process showed no observable influences on the UCPL properties of bare Tm@2.1 NPs. (**a–d**) Optical bright field (BF) (**a, b**) and SEM (**c, d**) images of Tm@2.1 NPs before (**a, c**) and after (**b, d**) the etching treatment. Scale bars: 10 μm. (**e**) The UCPL spectra for the Tm@2.1 NPs before (**a**) and after (**b**) the etching treatment. The optical signals were collected from the samples inside the circled area in (**a)** and (**b**).

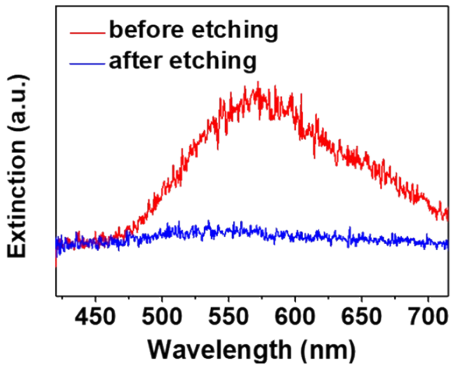

Figure S12. The scattering spectra of a single Tm@2.1/AgNW sample before (red) and after (blue) the selective etching process.

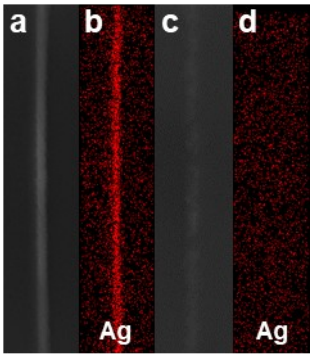

Figure S13. **The SEM and EDX mapping images of a single Tm@2.1/AgNW sample before and after the selective etching process.** (**a**, **b**) SEM (**a**) and EDX mapping (**b**) images of a pristine single Tm@2.1/AgNW sample before etching. (**c**, **d**) SEM (**c**) and EDX mapping (**d**) images of the Tm@2.1/AgNW sample after the selective etching process.

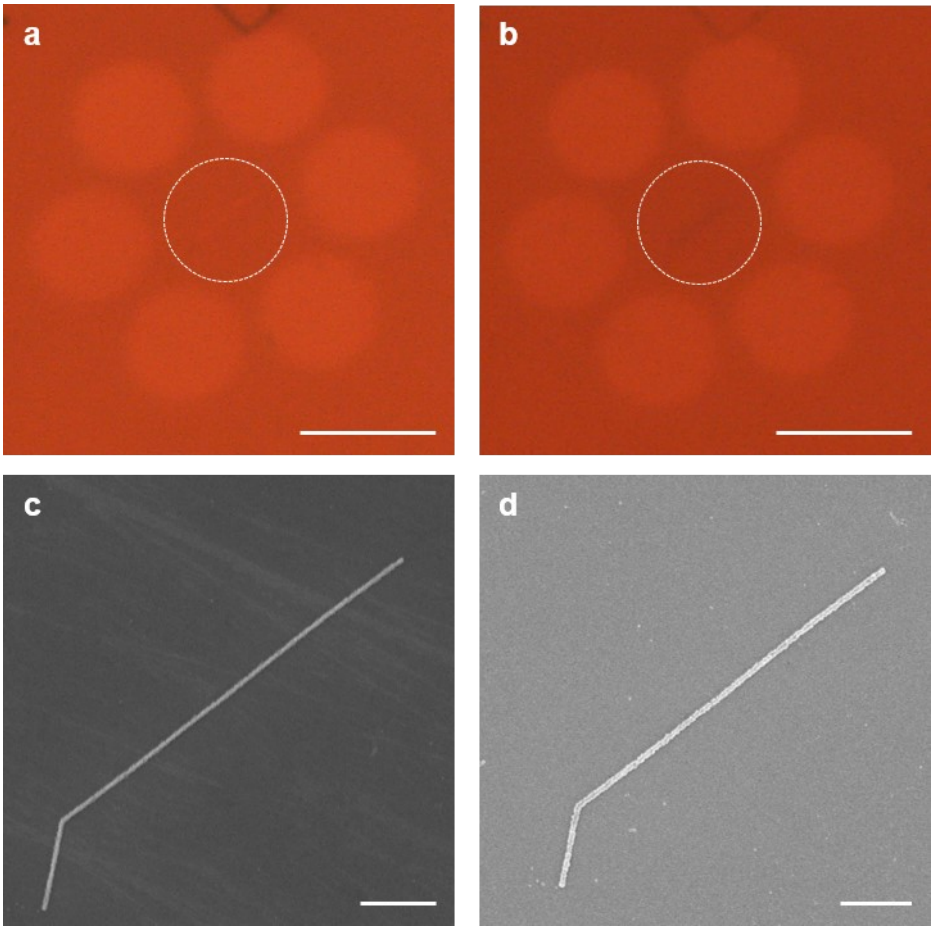

Figure S14. Optical BF and SEM images of one hybrid nanowire of Tm@2.1/AgNW (diameter: 55 nm) before and after etching. (**a**, **b**) Optical BF images of the hybrid nanowire of Tm@2.1/AgNW before (**a**) and after (**b**) etching. (**c**, **d**) SEM images of the hybrid nanowire of Tm@2.1/AgNW before (**c**) and after (**d**) etching. Scale bars: (**a**, **b**) 10 μm, (**c, d**) 1 μm.

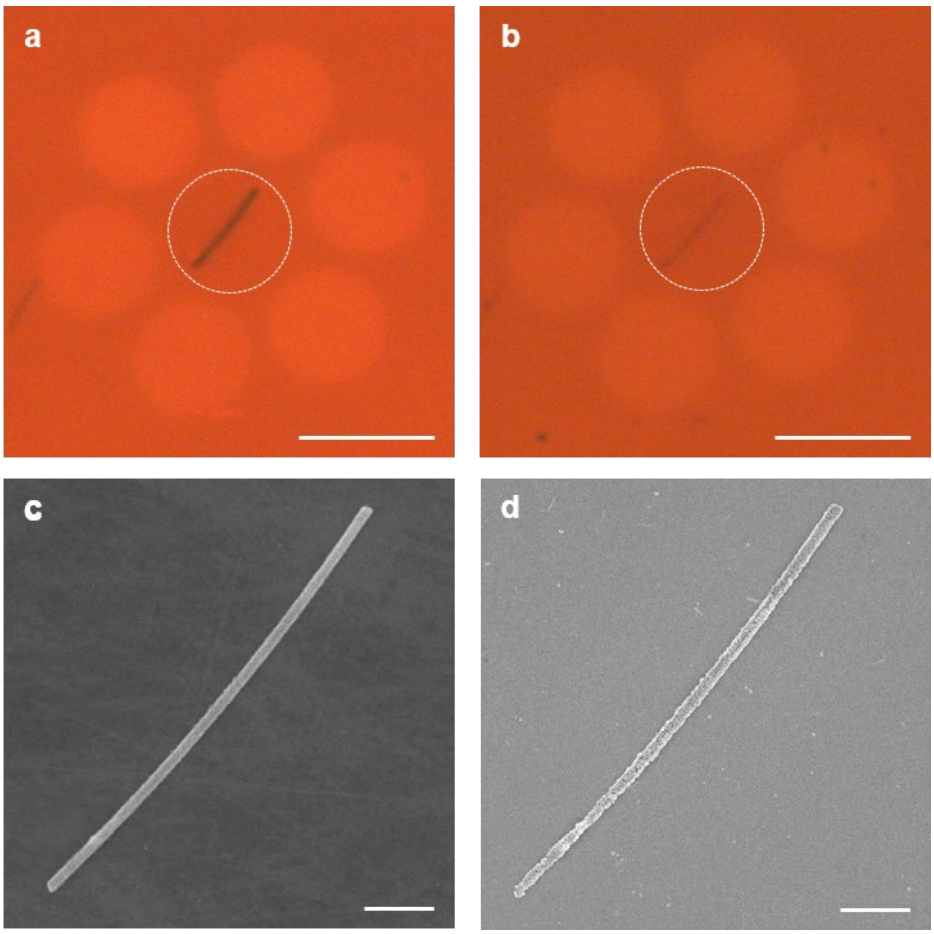

Figure S15. Optical BF and SEM images of one hybrid nanowire of Tm@2.1/AgNW (diameter: 164 nm) before and after etching. (**a**, **b**) Optical BF images of the hybrid nanowire of Tm@2.1/AgNW before (**a**) and after (**b**) etching. (**c**, **d**) SEM images of the hybrid nanowire of Tm@2.1/AgNW before (**c**) and after (**d**) etching. Scale bars: (**a**, **b**) 10 μm, (**c**, **d**) 1 μm.

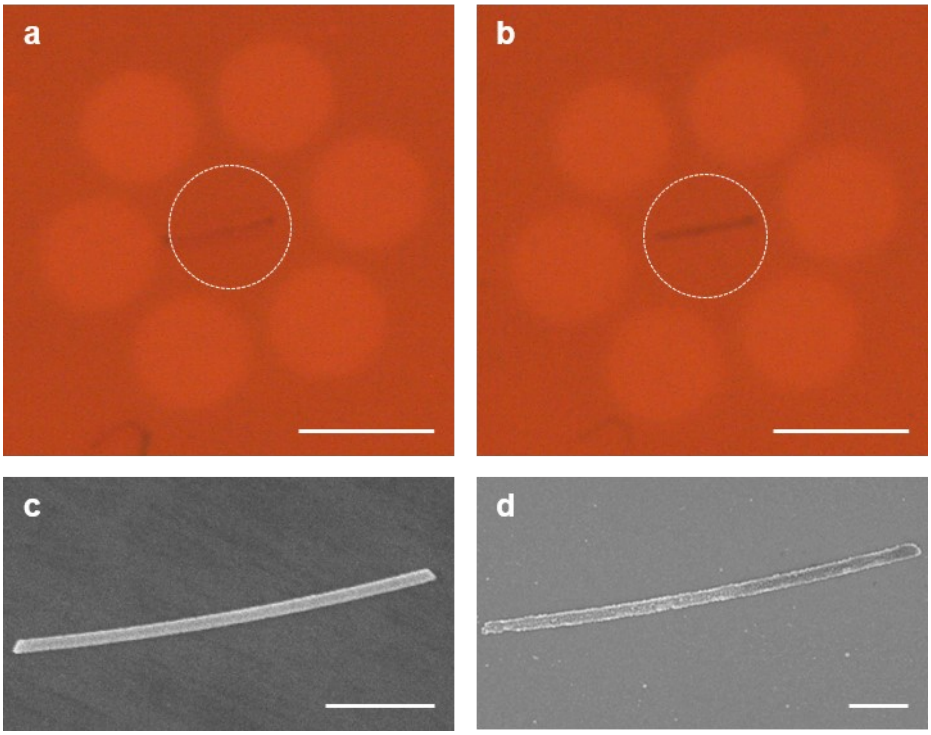

Figure S16. Optical BF and SEM images of one hybrid nanowire of Tm@2.1/AgNW (diameter: 208 nm) before and after etching. (**a**, **b**) Optical BF images of the hybrid nanowire of Tm@2.1/AgNW before (**a**) and after (**b**) etching. (**c**, **d**) SEM images of the hybrid nanowire of Tm@2.1/AgNW before (**c**) and after (**d**) etching. Scale bars: (**a**, **b**) 10 μm, (**c**) 2 μm, (**d**) 1 μm.

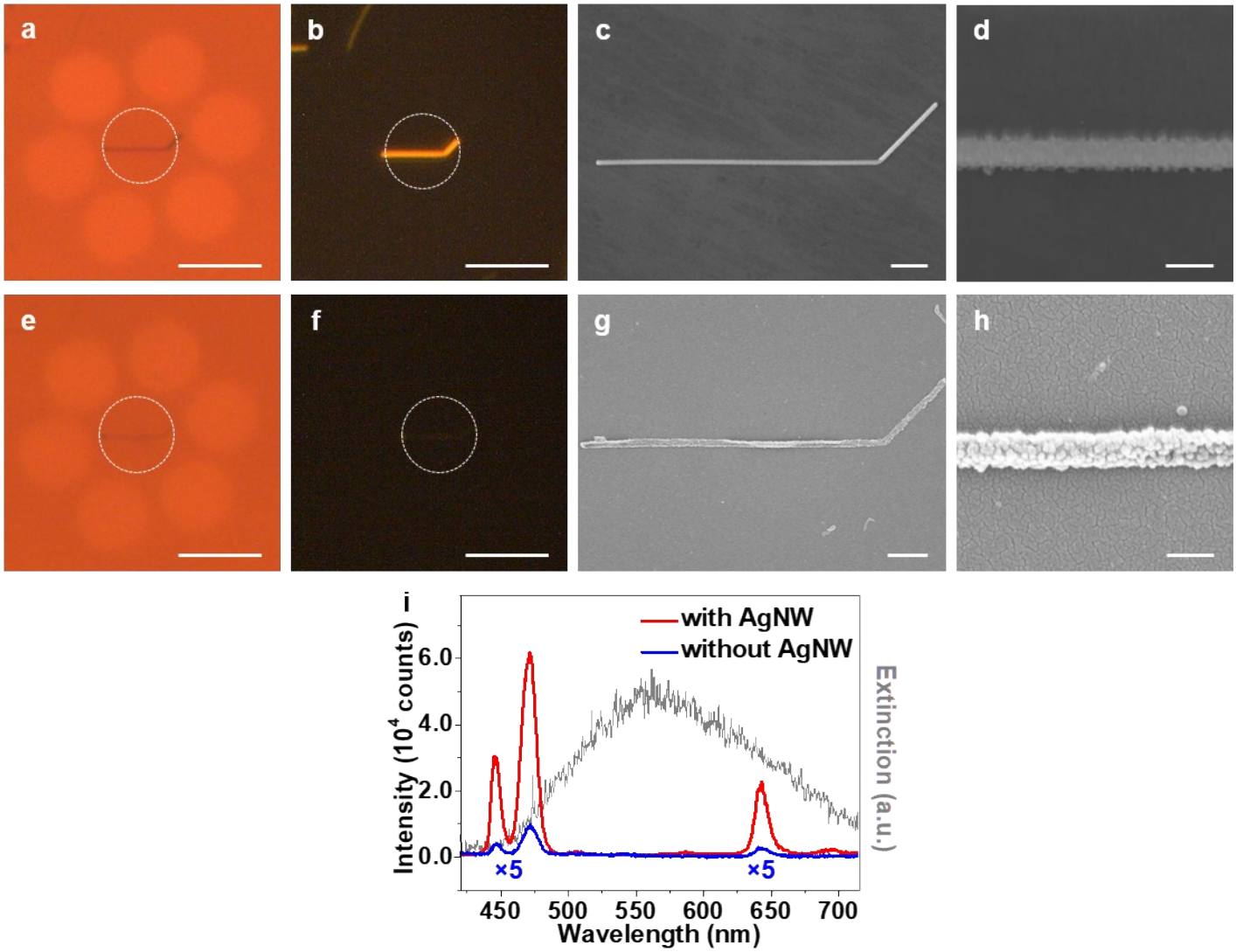

Figure S17. LSPR-enhanced UCPL performance for one hybrid nanowire of Tm@2.1/AgNW (diameter: 104 nm). (**a**–**d**) Optical BF (**a**), DF (**b**), and SEM (**c**, **d**) images of the hybrid nanowire of Tm@2.1/AgNW before etching. (**e**–**h**) Optical BF (**e**), DF (**f**), and SEM (**g**, **h**) images of the hybrid nanowire of Tm@2.1/AgNW after etching. Scale bars: (**a**, **b**, **e, f**) 10 μm, (**c**, **g**) 1 μm, (**d**, **h**) 200 nm. (**i**) The UCPL spectra for the Tm@2.1/AgNW before (red) and after (blue) selective etching (left axis), and the extinction spectrum (grey) for the Tm@2.1/AgNW before etching (right axis).

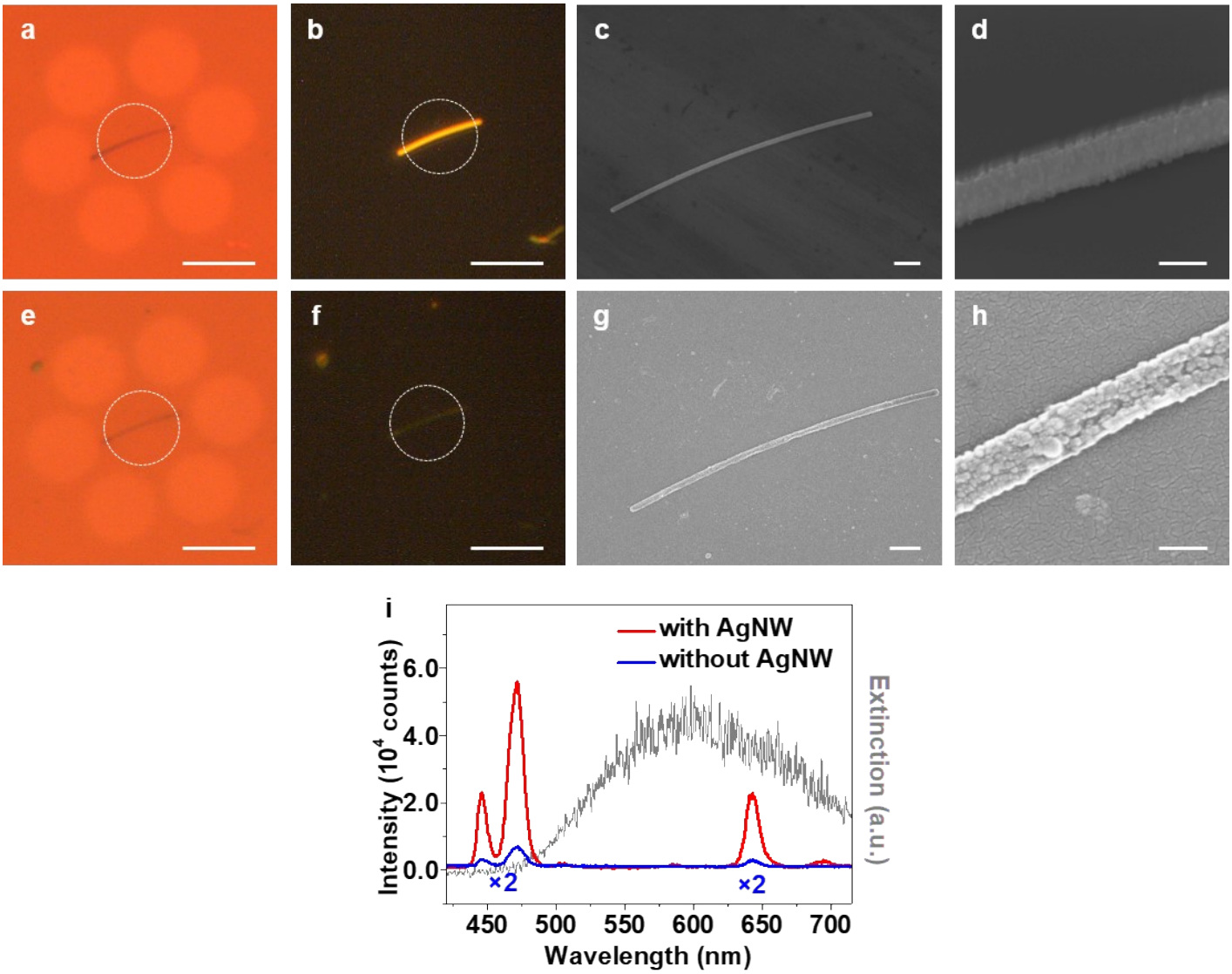

Figure S18. LSPR-enhanced UCPL performance for one hybrid nanowire of Tm@2.1/AgNW (diameter: 158 nm). (**a**–**d**) Optical BF (**a**), DF (**b**), and SEM (**c**, **d**) images of the hybrid nanowire of Tm@2.1/AgNW before etching. (**e**–**h**) Optical BF (**e**), DF (**f**), and SEM (**g**, **h**) images of the hybrid nanowire of Tm@2.1/AgNW after etching. Scale bars: (**a**, **b**, **e, f**) 10 μm, (**c**, **g**) 1 μm, (**d**, **h**) 200 nm. (**i**) The UCPL spectra for the Tm@2.1/AgNW before (red) and after (blue) etching (left axis), and the extinction spectrum (grey) for the Tm@2.1/AgNW before etching (right axis).

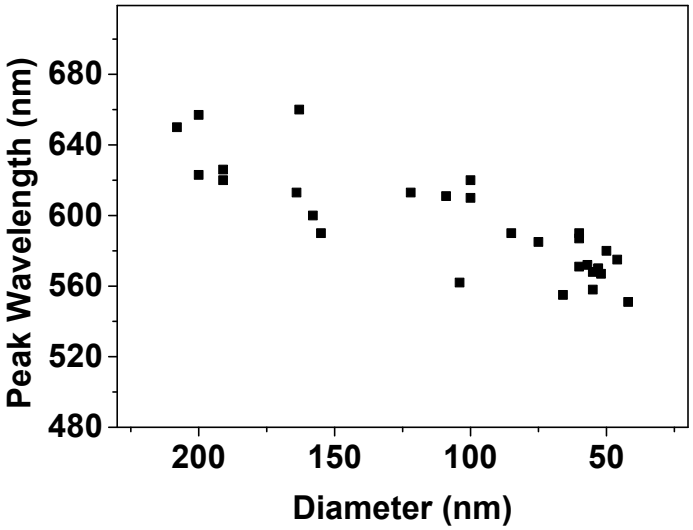

Figure S19 The quantitative statistics showing the dependence of the scattering peak wavelength on the diameter of AgNWs.

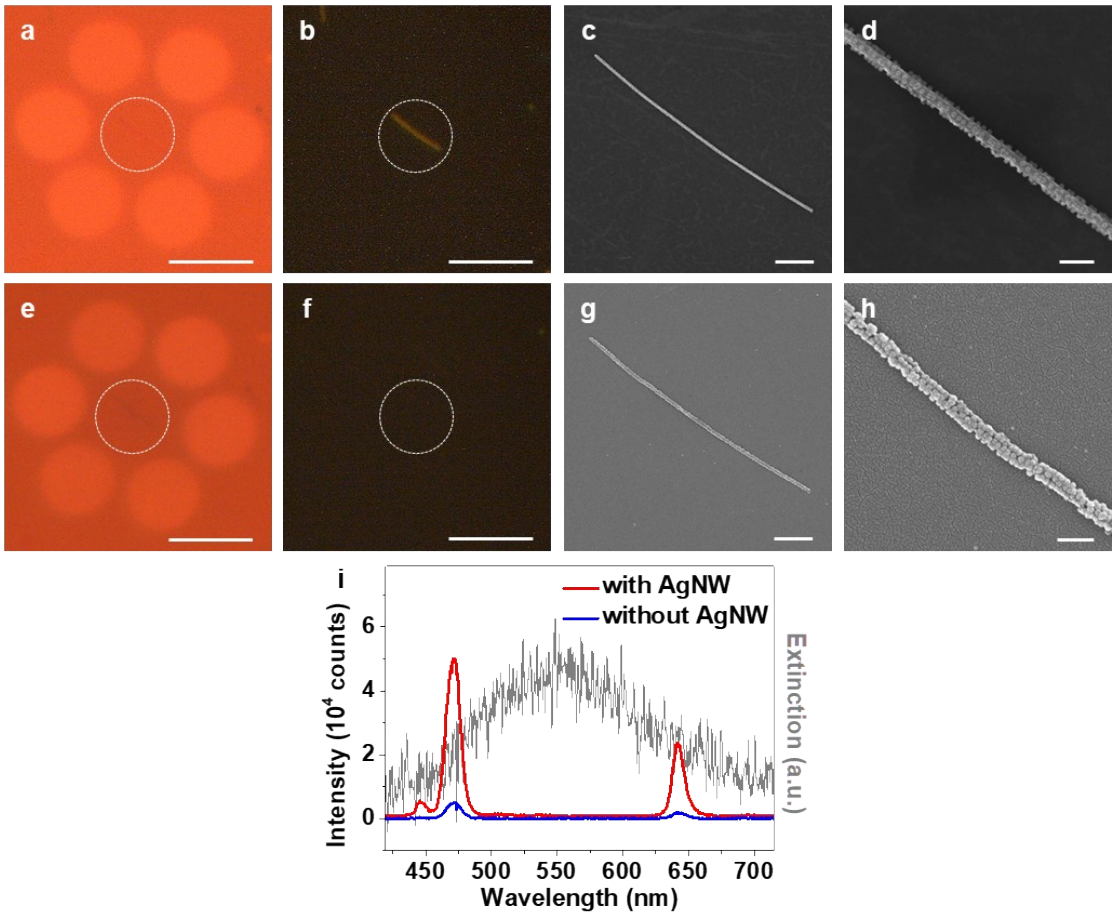

Figure S20. LSPR-enhanced UCPL performance for one hybrid nanowire of 0.5%Tm@2.6/AgNW (diameter: 66 nm). (**a**–**d**) Optical BF (**a**), DF (**b**), and SEM (**c**, **d**) images of the hybrid nanowire of 0.5%Tm@2.6/AgNW before etching. (**e**–**h**) Optical BF (**e**), DF (**f**), and SEM (**g**, **h**) images of the hybrid nanowire of 0.5%Tm@2.6/AgNW after etching. Scale bars: (**a**, **b**, **e, f**) 10 μm, (**c**, **g**) 1 μm, (**d**, **h**) 200 nm. (**i**) The UCPL spectra for the 0.5%Tm@2.6/AgNW before (red) and after (blue) selective etching (left axis), and the extinction spectrum (grey) for the 0.5%Tm@2.6/AgNW before etching (right axis). The single AgNW resulted in 10-fold increase of the UCPL intensity of 0.5%Tm@2.6/AgNW.

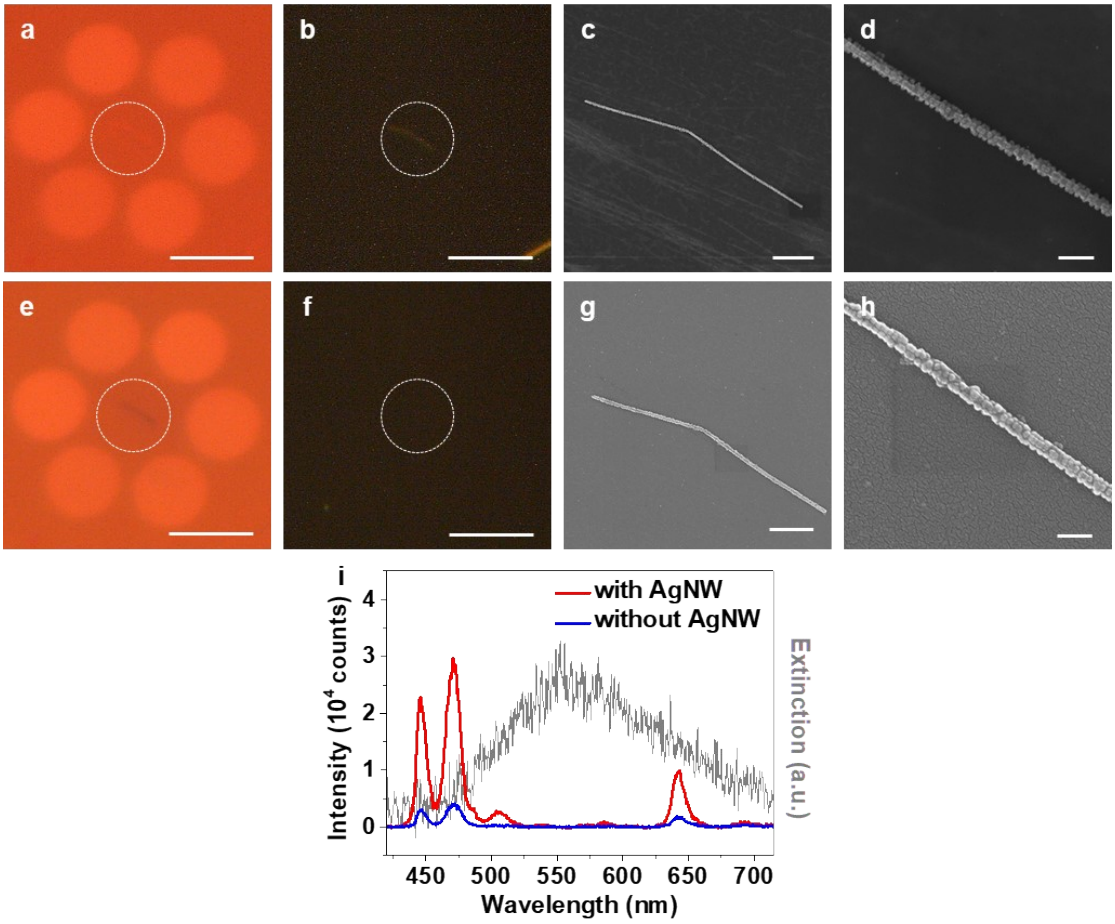

Figure S21. LSPR-enhanced UCPL performance for one hybrid nanowire of 1.5%Tm@2.6/AgNW (diameter: 41 nm). (**a**–**d**) Optical BF (**a**), DF (**b**), and SEM (**c**, **d**) images of the hybrid nanowire of 1.5%Tm@2.6/AgNW before etching. (**e**–**h**) Optical BF (**e**), DF (**f**), and SEM (**g**, **h**) images of the hybrid nanowire of 1.5%Tm@2.6/AgNW after etching. Scale bars: (**a**, **b**, **e, f**) 10 μm, (**c**, **g**) 1 μm, (**d**, **h**) 200 nm. (**i**) The UCPL spectra for the 1.5%Tm@2.6/AgNW before (red) and after (blue) selective etching (left axis), and the extinction spectrum (grey) for the 1.5%Tm@2.6/AgNW before etching (right axis). The single AgNW resulted in 8-fold increase of the UCPL intensity of 1.5%Tm@2.6/AgNW.

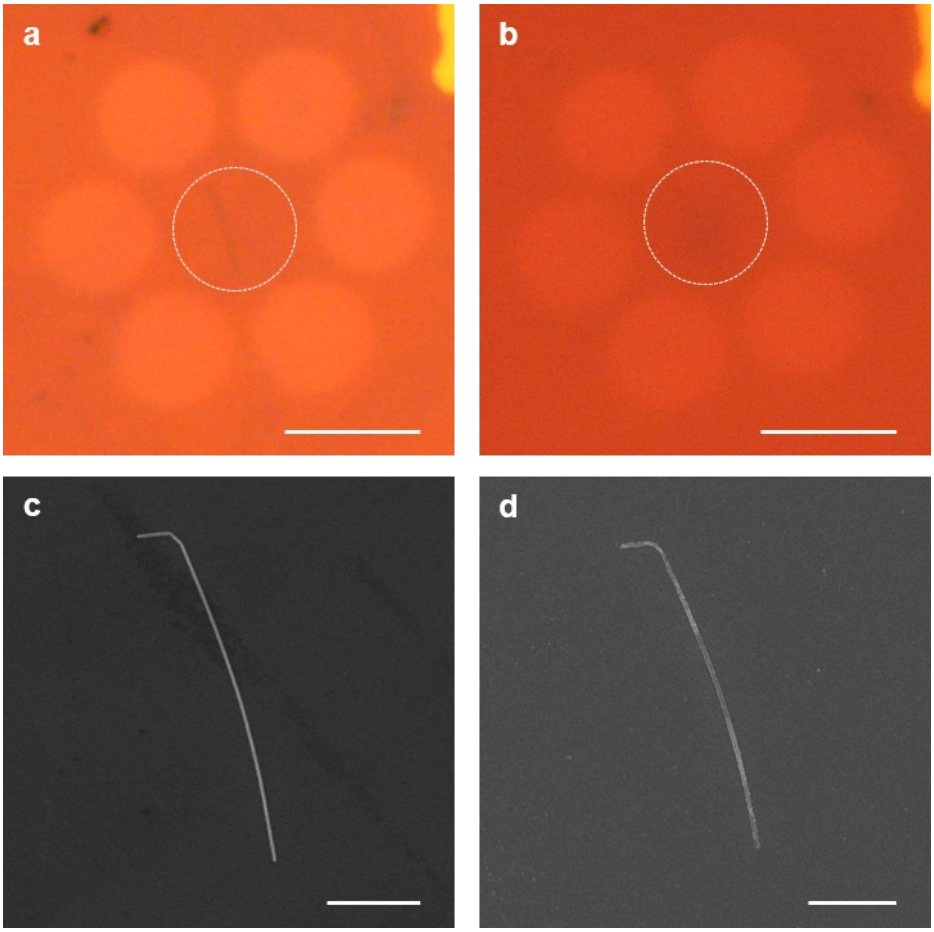

Figure S22. Optical BF and SEM images of one hybrid nanowire of Er@2.6/AgNW (diameter: 53 nm) before and after etching. (**a**, **b**) Optical BF images of the hybrid nanowire of Er@2.6/AgNW before (**a**) and after (**b**) etching. (**c**, **d**) SEM images of the hybrid nanowire of Er@2.6/AgNW before (**c**) after (**d**) etching. Scale bars: (**a**, **b**) 10 μm, (**c**, **d**) 2 μm.

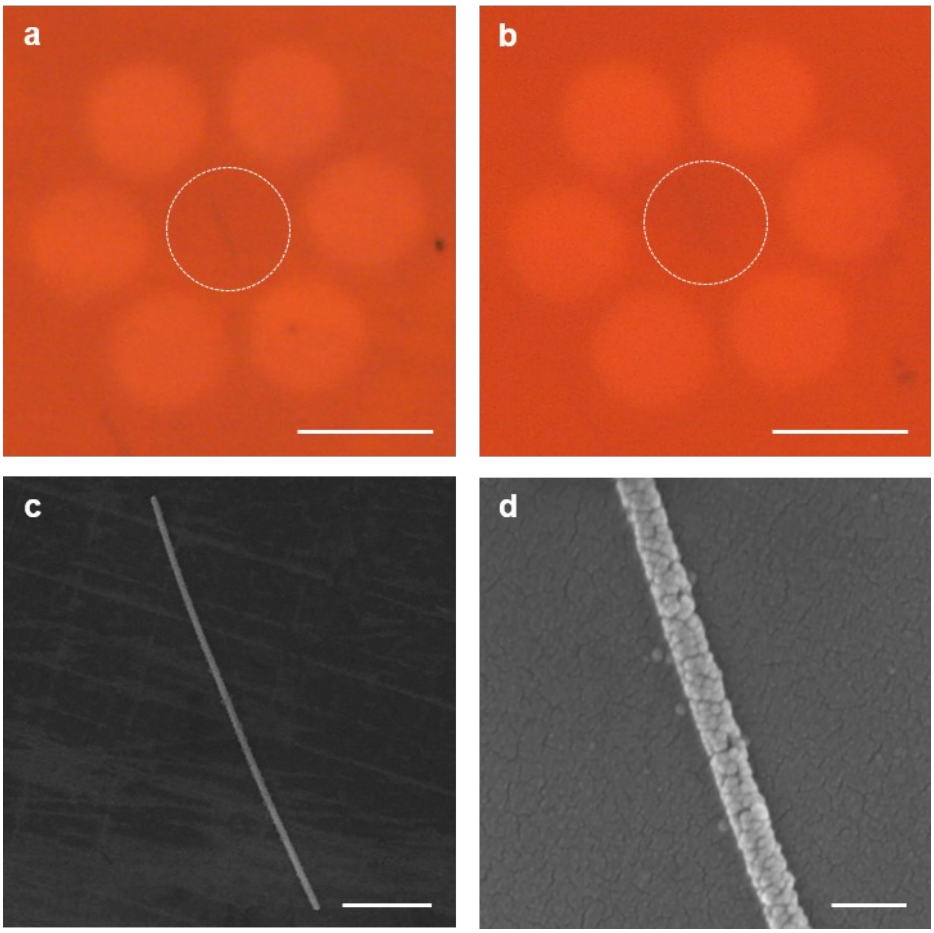

Figure S23. Optical BF and SEM images for one hybrid nanowire of Er@2.6/AgNW (diameter: 60 nm) before and after etching. (**a**, **b**) Optical BF images of the hybrid nanowire of Er@2.6/AgNW before (**a**) and after (**b**) etching. (**c**, **d**) SEM images of the hybrid nanowire of Er@2.6/AgNW before (**c**) after (**d**) etching. Scale bars: (**a**, **b**) 10 μm, (**c**) 1 μm, (**d**) 200 nm.

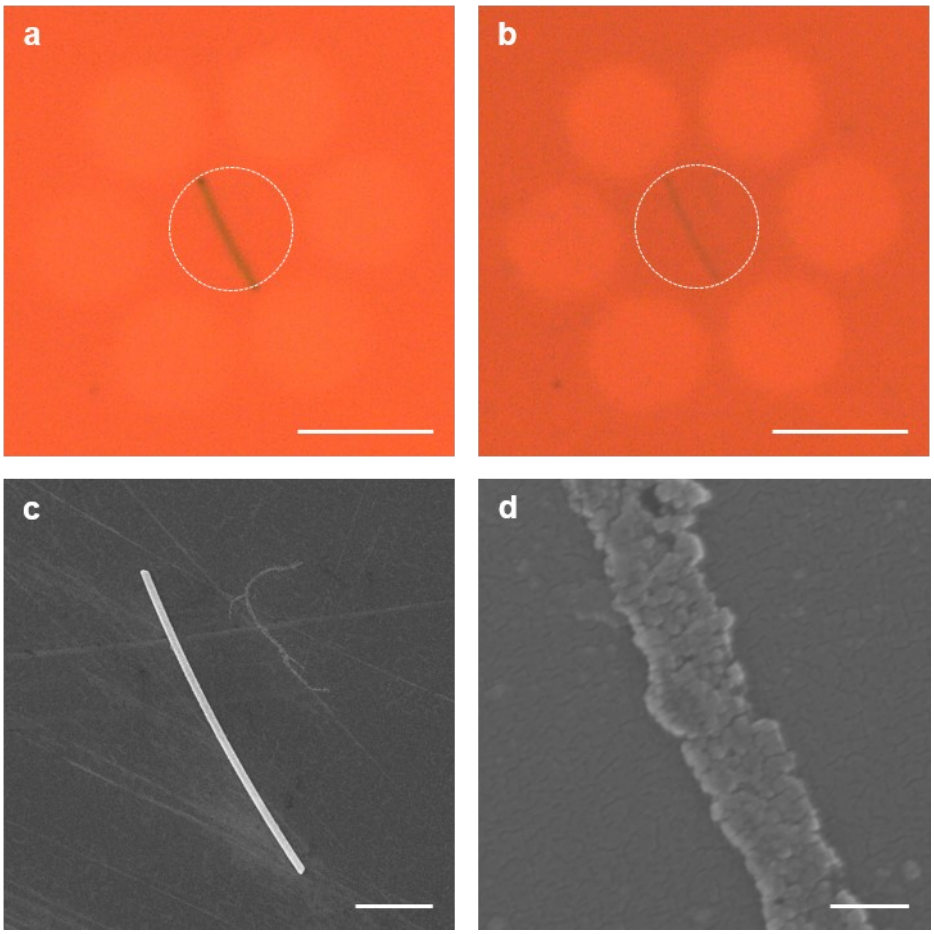

Figure S24. Optical BF and SEM images of one hybrid nanowire of Er@2.6/AgNW (diameter: 200 nm) before and after etching. (**a**, **b**) Optical BF images of the hybrid nanowire of Er@2.6/AgNW before (**a**) and after (**b**) etching. (**c**, **d**) SEM images of the hybrid nanowire of Er@2.6/AgNW before (**c**) and after (**d**) etching. Scale bars: (**a**, **b**) 10 μm, (**c**) 2 μm, (**d**) 200 nm.

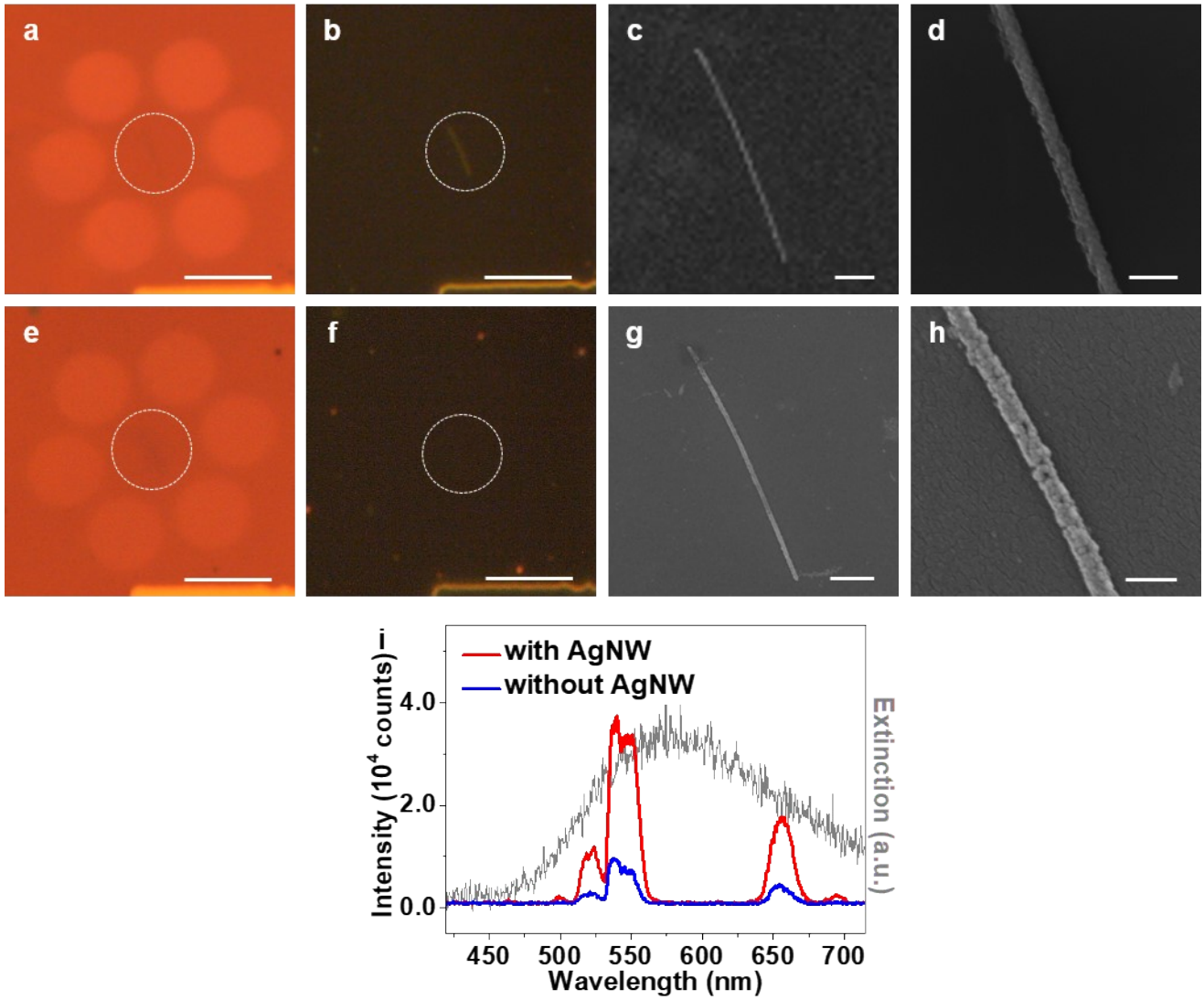

Figure S25. LSPR-enhanced UCPL performance for one hybrid nanowire of Er@2.6/AgNW (diameter: 46 nm). (**a**–**d**) Optical BF (**a**), DF (**b**), and SEM (**c**, **d**) images of the hybrid nanowire of Er@2.6/AgNW before etching. (**e**–**h**) Optical BF (**e**), DF (**f**), and SEM (**g**, **h**) images of the hybrid nanowire of Er@2.6/AgNW after etching. Scale bars: (**a**, **b**, **e**, **f**) 10 μm, (**c**, **g**) 1 μm, (**d**, **h**) 200 nm. (**i**) The UCPL spectra for the Er@2.6/AgNW before (red) and after (blue) selective etching (left axis), and the extinction spectrum (grey) for the Er@2.6/AgNW before etching (right axis).

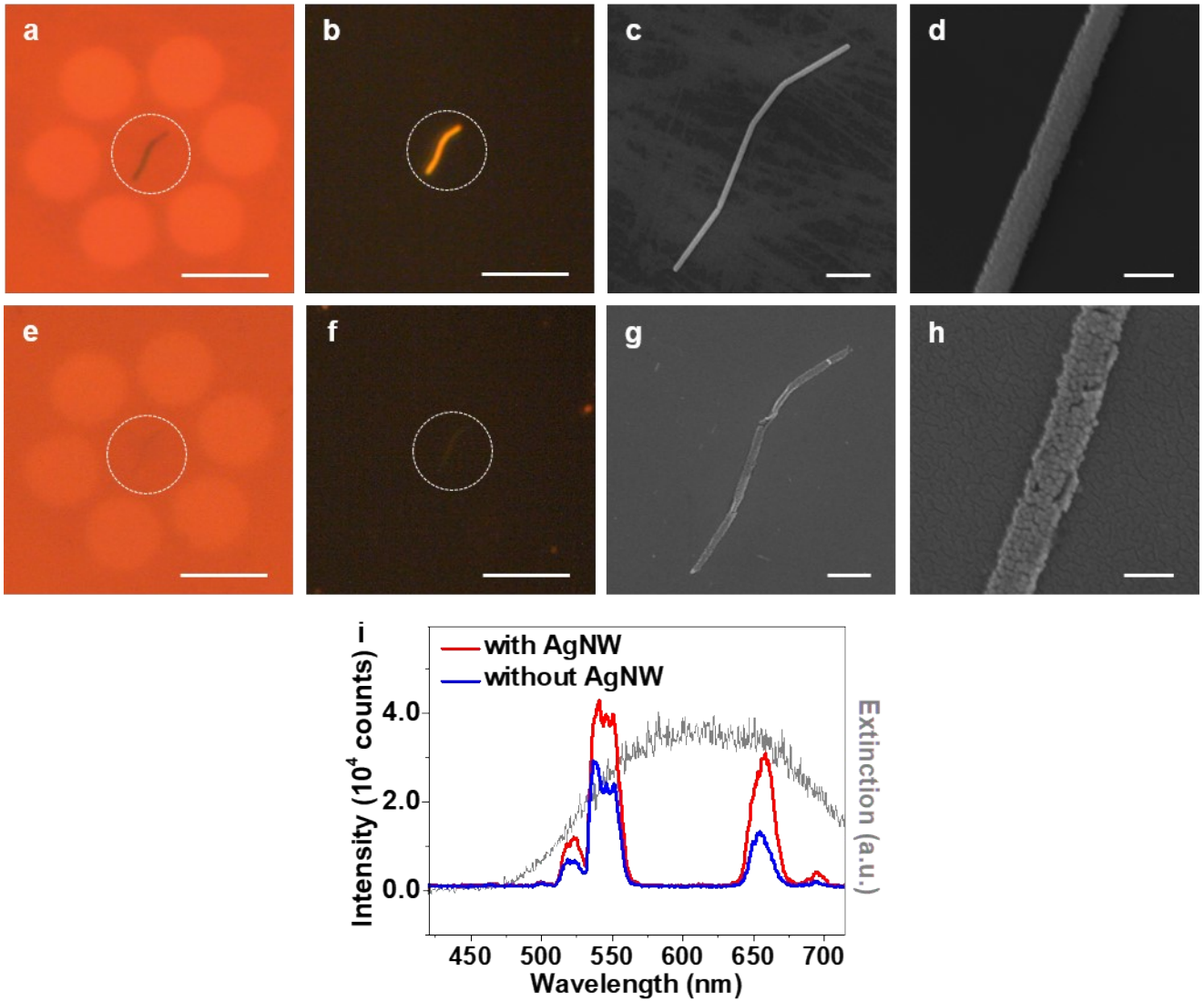

Figure S26. LSPR-enhanced UCPL performance for one hybrid nanowire of Er@2.6/AgNW (diameter: 100 nm). (**a**–**d**) Optical BF (**a**), DF (**b**), and SEM (**c**, **d**) images of the hybrid nanowire of Er@2.6/AgNW before etching. (**e**–**h**) Optical BF (**e**), DF (**f**), and SEM (**g**, **h**) images of the hybrid nanowire of Er@2.6/AgNW after etching. Scale bars: (**a**, **b**, **e**, **f**) 10 μm, (**c**, **g**) 1 μm, (**d**, **h**) 200 nm. (**i**) The UCPL spectra for the Er@2.6/AgNW before (red) and after (blue) selective etching (left axis), and the extinction spectrum (grey) for the Er@2.6/AgNW before etching (right axis).

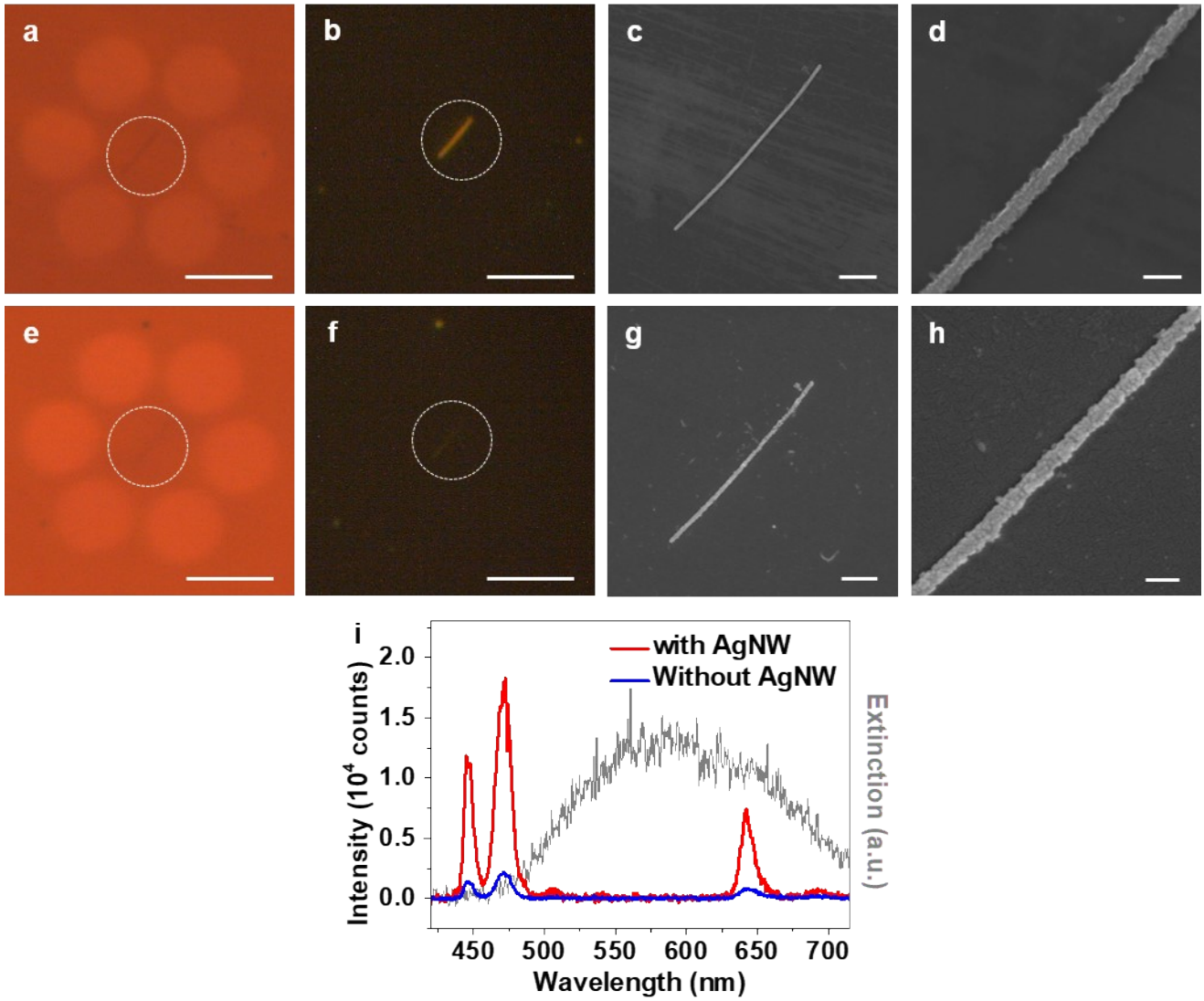

Figure S27. LSPR-enhanced UCPL performance for one hybrid nanowire of uncoated *β*-Tm/AgNW (diameter: 67 nm). (**a**–**d**) Optical BF (**a**), DF (**b**), and SEM (**c**, **d**) images of the hybrid nanowire of *β*-Tm/AgNW before etching. (**e**–**h**) Optical BF (**e**), DF (**f**), and SEM (**g**, **h**) images of the hybrid nanowire of *β*-Tm/AgNW after etching. Scale bars: (**a**, **b**, **e**, **f**) 10 μm, (**c**, **g**) 1 μm, (**d**, **h**) 200 nm. (**i**) The UCPL spectra for the uncoated *β*-Tm/AgNW before (red) and after (blue) selective etching (left axis), and the extinction spectrum (grey) for the uncoated *β*-Tm/AgNW before etching (right axis). The single AgNW just resulted in 8-fold increase of the UCPL intensity of *β*-Tm/AgNW.

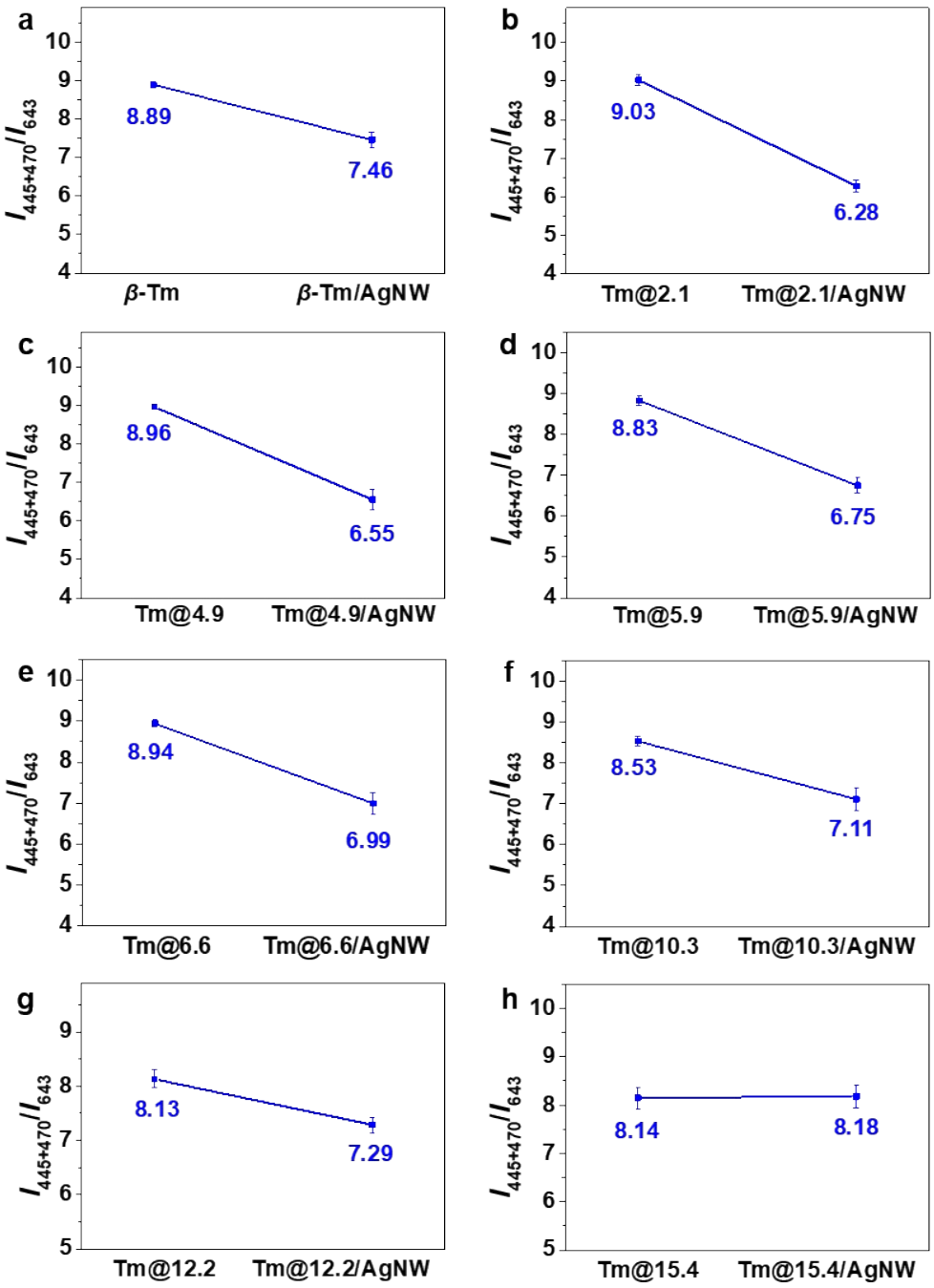

Figure S28. Distance-dependent LSPR-UCPL coupling behavior for Tm-doped UCNPs/AgNWs, in which AgNW with diameters of 170–200 nm and lengths of 7–8.5 μm. The comparison chart of the $I_{445+470}/I_{643}$ ratios of Tm-doped UCNP UCNPs (with different $NaYF_4$ shell thicknesses) with and without single AgNW: (**a**) uncoated *β*-Tm/AgNWs, (**b**) Tm@2.1/AgNWs, (**c**) Tm@4.9/AgNWs, (**d**) Tm@5.9/AgNWs, (**e**) Tm@6.6/AgNWs, (**f**) Tm@10.3/AgNWs, (**g**) Tm@12.2/AgNWs, (**h**) Tm@15.4/AgNWs. The error bars for pure Tm-doped UCNPs and Tm-doped UCNPs/AgNWs indicated the standard deviation for five and fifteen independent samples tested on Si substrate, respectively.

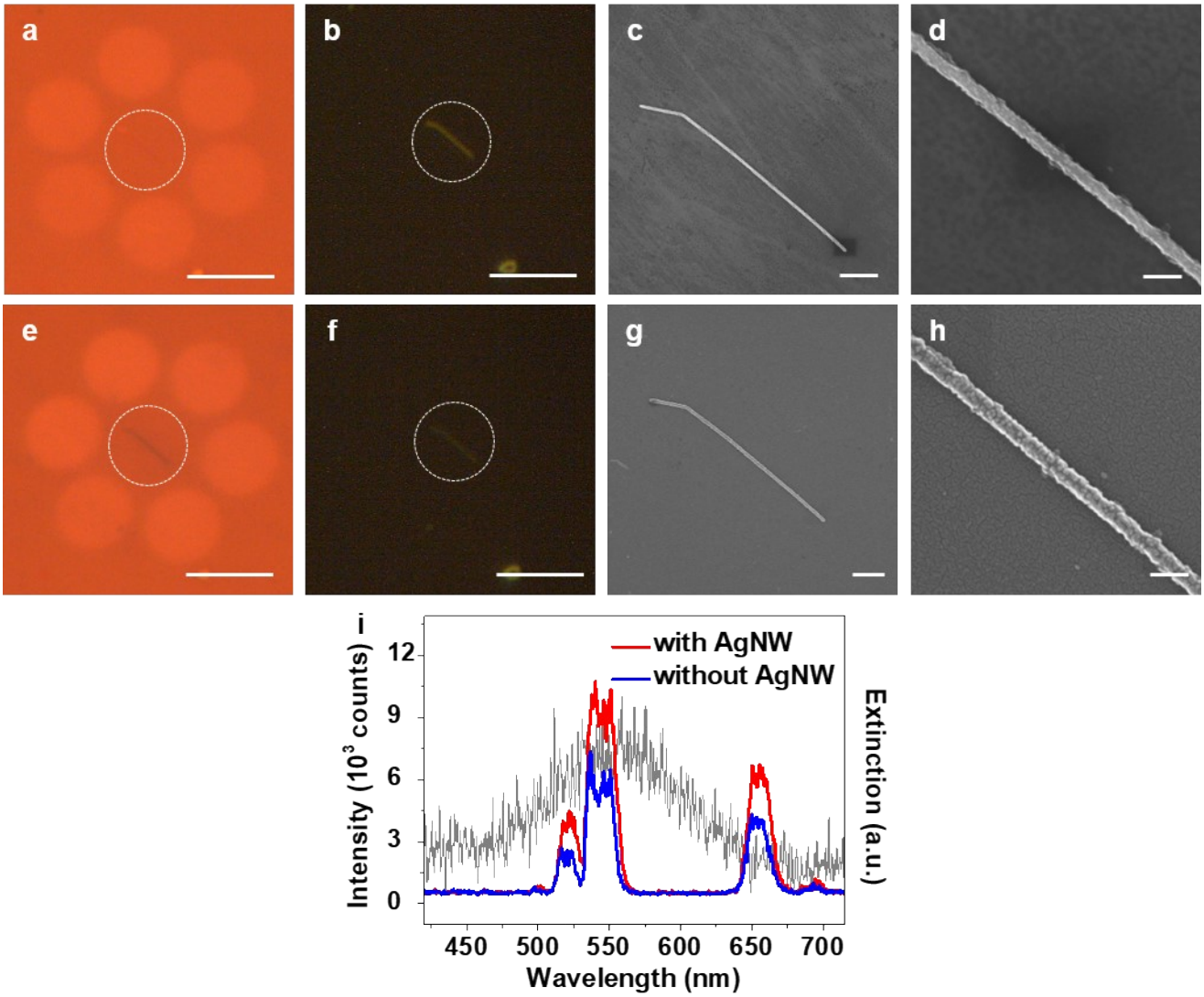

Figure S29. LSPR-enhanced UCPL performance for one hybrid nanowire of uncoated *β*-Er/AgNW (diameter: 54 nm). (**a**–**d**) Optical BF (**a**), DF (**b**), and SEM (**c**, **d**) images of the hybrid nanowire of *β*-Er/AgNW before etching. (**e**–**h**) Optical BF (**e**), DF (**f**), and SEM (**g**, **h**) images of the hybrid nanowire of *β*-Er/AgNW after etching. Scale bars: (**a**, **b**, **e**, **f**) 10 μm, (**c**, **g**) 1 μm, (**d**, **h**) 200 nm. (**i**) The UCPL spectra for the uncoated *β*-Er/AgNW before (red) and after (blue) selective etching (left axis), and the extinction spectrum (grey) for the uncoated *β*-Er/AgNW before etching (right axis). The single AgNW just resulted in 2-fold increase of the UCPL intensity of *β*-Er/AgNW.

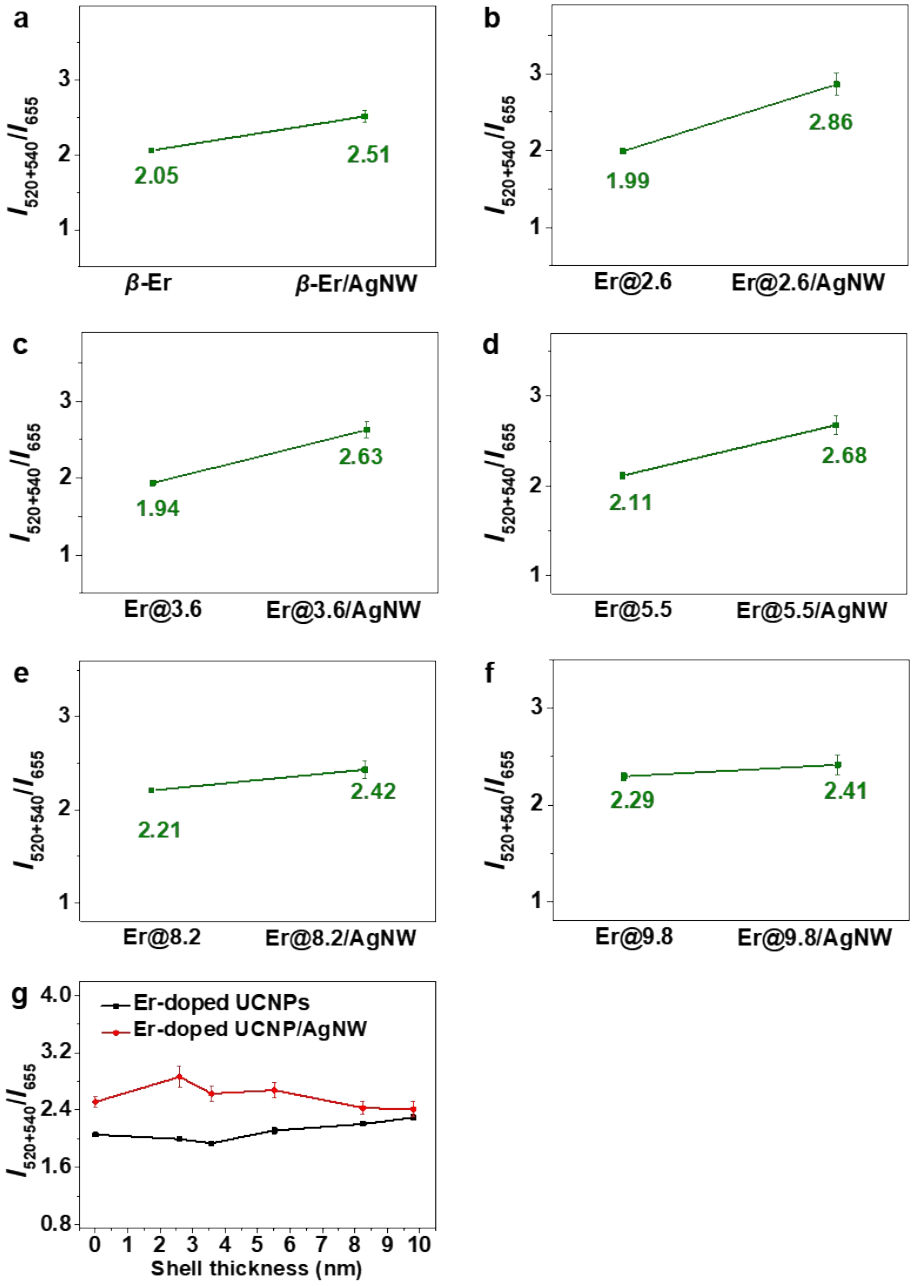

Figure S30. Distance-dependent LSPR-UCPL coupling behavior for Er-doped UCNPs/AgNWs, in which AgNWs with diameters of 80–100 nm and lengths of 8–10 μm. (**a**–**f**) The comparison chart of the $I_{520+540}/I_{655}$ ratios of Er-doped UCNPs (with different $NaYF_4$ shell thicknesses) with and without single AgNW: (**a**) uncoated *β*-Er/AgNWs, (**b**) Er@2.6/AgNWs, (**c**) Er@3.6/AgNWs, (**d**) Er@5.5/AgNWs, (**e**) Er@8.2/AgNWs, (**f**) Er@9.8/AgNWs. (**g**) The $I_{520+540}/I_{655}$ ratios for upconversion emissions of the Er-doped UCNPs with different $NaYF_4$ shell thicknesses (black) and their corresponding hybrids with AgNWs (i.e., UCNPs/AgNWs) (red). The error bars indicated the standard deviation for five and fifteen independent samples for the UCNPs and UCNPs/AgNWs, respectively.

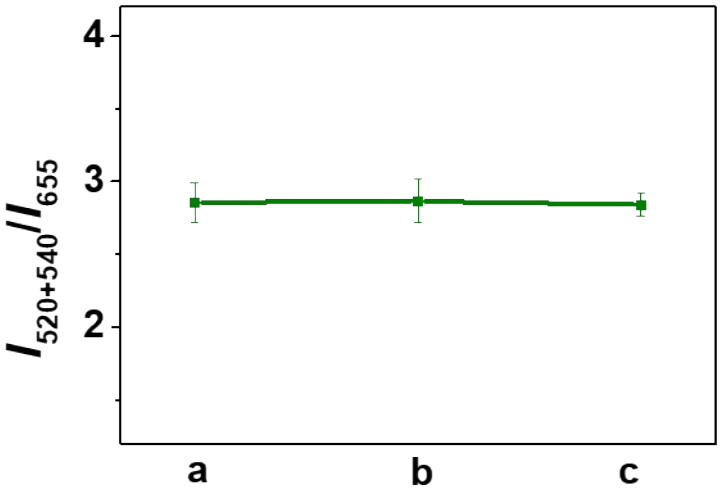

Figure S31. LSPR-UCPL coupling behavior for Er@2.6/AgNW with varied coverages. The statistical $I_{520+540}/I_{655}$ ratios for single Er@2.6/AgNW hybrids shown in Figure S7. The error bars indicated the standard deviation for fifteen independent samples.

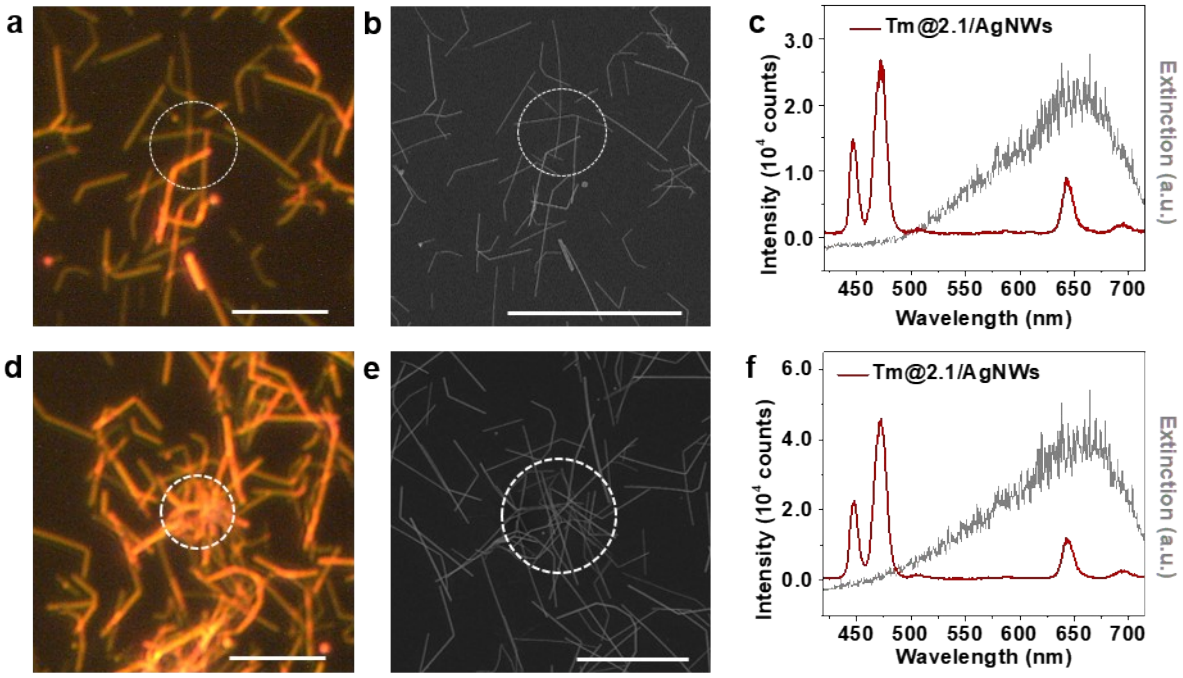

g

	exposure time	I_{445}/I_{643}	I_{470}/I_{643}
c	1 s	1.22	3.33
f	0.001 s	1.42	4.17

Figure S32. LSPR-UCPL coupling behavior for randomly aggregated Tm@2.1/AgNWs. (**a**, **b**) Optical DF and SEM images for amounts of Tm@2.1/AgNWs. (**c**) The UCPL (red) and extinction (grey) spectra for Tm@2.1/AgNWs shown in (a, b). (**d**–**f**) The optical DF (**d**), SEM (**e**), and UCPL spectrum (**f**) of another site of Tm@2.1/AgNWs on the same substrate. Scale bars: (**a**, **d**) 20 μm. (**b**, **e**) 10 μm. (**g**) The I_{445}/I_{643} and I_{470}/I_{643} ratios for the abovementioned Tm@2.1/AgNWs.

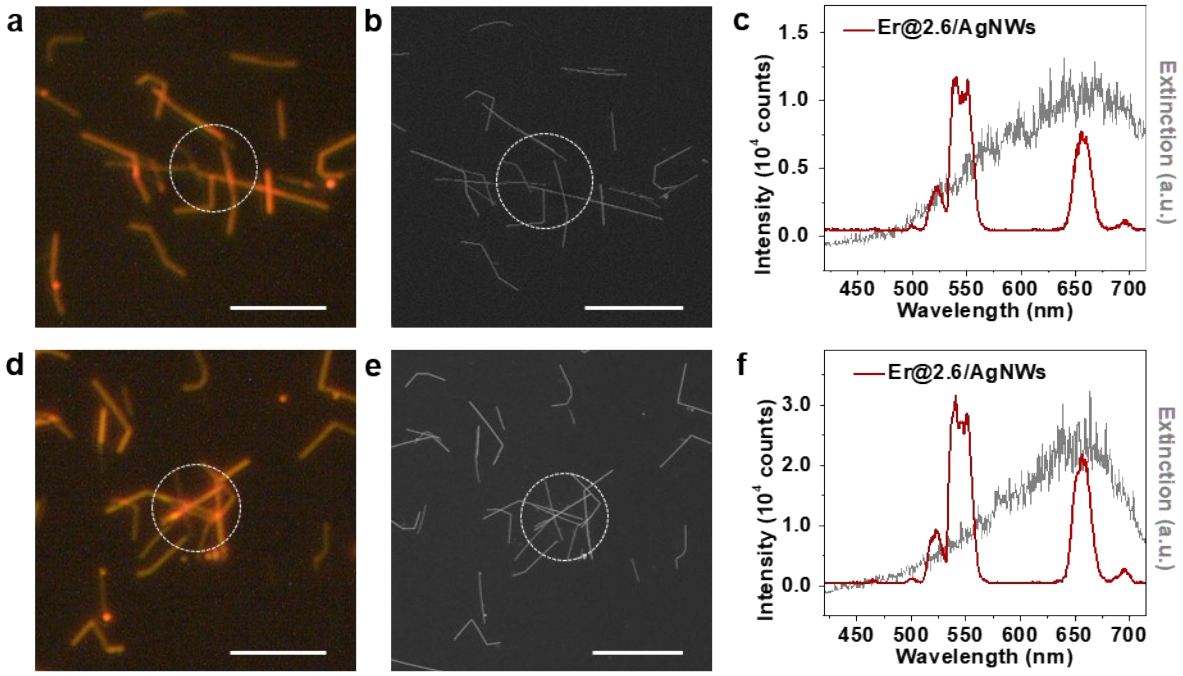

g

	exposure time	I_{520}/I_{655}	I_{540}/I_{655}
c	0.001 s	0.31	1.81
f	0.001 s	0.3	1.62

Figure S33. LSPR-UCPL coupling behavior for randomly aggregated Er@2.6/AgNWs. (**a**, **b**) Optical DF and SEM images of amounts of Er@2.6/AgNWs. (**c**) The UCPL (red) and extinction (grey) spectra for Er@2.6/AgNWs. (**d**–**f**) The optical DF (**d**), SEM (**e**), and UCPL spectrum (**f**) of another site of Er@2.6/AgNWs on the same substrate. Scale bars: (**a**, **d**) 20 μm. (**b**, **e**) 10 μm. (**g**) The I_{520}/I_{655} and I_{540}/I_{655} ratios for the abovementioned Er@2.6/AgNWs.

Table S1. The structure and optical parameters for Tm@2.1/AgNWs. Exposure Times (EXP Times), enhancement factors (EFs), the intensity ratios for the I_{445}/I_{643} and I_{470}/I_{643} of Tm@2.1/AgNWs before and after etching, the diameters of the AgNWs.

Sample (Figure)	Exp Times		EFs*			AgNW	I_{445}/I_{643}		I_{470}/I_{643}	
	before	after	445 (nm)	470 (nm)	643 (nm)	diameter (nm)	before	after	before	after
3e	5	45	21	14	13	55	1.10	0.67	3.58	3.20
S13i	5	45	54	36	36	104	1.01	0.67	3.11	3.08
S14i	5	45	25	19	24	158	0.70	0.67	2.57	3.14
3j	5	45	49	29	48	164	0.62	0.60	1.94	3.18
3o	5	45	25	23	48	208	0.4	0.78	1.8	3.8

*Enhancement factors from different samples were obtained by dividing photoluminescence intensity of the Tm@2.1/AgNW by those remaining Tm@2.1 UCNPs after etching.

Table S2. The structure and optical parameters for Er@2.6/AgNWs. Exposure Times (EXP Times), enhancement factors (EFs), the intensity ratios for the I_{520}/I_{655} and I_{540}/I_{655} of Er@2.6/AgNW before and after etching, the diameters of the AgNWs.

Sample (Figure)	Exp Times		EFs*			AgNW	I_{520}/I_{655}		I_{540}/I_{655}	
	before	after	520 (nm)	540 (nm)	655 (nm)	diameter (nm)	before	after	before	after
4e	1	1	5.3	4.5	4.8	53	0.49	0.38	2.57	2.28
S18i	1	1	5.4	4.8	5.2	46	0.48	0.39	2.49	2.24
4j	1	1	5.5	5.7	7.0	60	0.38	0.42	2.11	2.19
S19i	1	1	1.8	1.7	2.7	100	0.27	0.35	1.57	2.26
4o	0.5	0.5	2.1	1.8	4.5	200	0.2	0.38	1.11	2.37

*Enhancement factors from different samples were obtained by dividing photoluminescence intensity of the Er@2.6/AgNW by those remaining Er@2.6 UCNPs after etching.

REFERENCES

(1) P.-Z. Zhang, R. Liu, L.-D. Sun, H. Dong, L.-D. Li, X.-Y. Zheng, K. Wu and C.-H. Yan, *Inorg. Chem. Front*., 2018, **5**, 1800–1804.

(2) H. Dong, L.-D. Sun, Y.-F. Wang, J.-W. Xiao, D. T. Tu, X. Y. Chen and C.-H. Yan, *J. Mater. Chem. C*, 2016, **4**, 4186–4192.

(3) A. G. Dong, X. C. Ye, J. Chen, Y. J. Kang, T. Gordon, J. M. Kikkawa and C. B. Murray, *J. Am. Chem. Soc*., 2011, **133**, 998–1006.

(4) J. Jung, H. Lee, I. Ha, H. Cho, K. K. Kim, J. Kwon, P. Won, S. Hong and S. H. Ko, *ACS Appl. Mater. Inter*., 2017, **9**, 44609–44616.

(5) X. L. Zhuo, X. Z. Zhu, Q. Li, Z. Yang and J. F. Wang, *ACS Nano*, 2015, **9**, 7523–7535.